UNIVERSIDADE FEDERAL DE PERNAMBUCO
DEPARTAMENTO DE FÍSICA – CCEN
PROGRAMA DE PÓS-GRADUAÇÃO EM FÍSICA

ÁLVARO MITCHELL GALVÃO DE MELO

FORWARD FOUR-WAVE MIXING VIA RECOIL-INDUCED RESONANCES IN COLD CESIUM ATOMS

Recife
2019

ÁLVARO MITCHELL GALVÃO DE MELO

FORWARD FOUR-WAVE MIXING VIA RECOIL-INDUCED RESONANCES IN COLD CESIUM ATOMS

Dissertação apresentada ao Programa de Pós-Graduação em Física da Universidade Federal de Pernambuco, como requisito parcial para a obtenção do título de Mestre em Física.

Área de Concentração: Óptica

Orientador: Prof. José Wellington Rocha Tabosa

Recife
2019

Catalogação na fonte
Bibliotecária Arabelly Ascoli CRB4-2068

M528f Melo, Álvaro Mitchell Galvão de
Forward four-wave mixing via recoil-induced resonances in cold cesium atoms / Álvaro Mitchell Galvão de Melo. – 2019.
59 f.: il., fig.

Orientador: José Wellington Rocha Tabosa
Dissertação (Mestrado) – Universidade Federal de Pernambuco. CCEN. Física. Recife, 2019.
Inclui referências.

1. Óptica. 2. Ressonâncias induzidas por recuo. 3. Armadilha magneto-óptica. 4. Física atômica. I. Tabosa, José Wellington Rocha (orientador). II. Título.

535.2 CDD (22. ed.) UFPE-CCEN 2020-32

ÁLVARO MITCHELL GALVÃO DE MELO

FORWARD FOUR-WAVE MIXING VIA RECOIL-INDUCED RESONANCES IN COLD CESIUM ATOMS

Dissertação apresentada ao Programa de Pós-Graduação em Física da Universidade Federal de Pernambuco, como requisito parcial para a obtenção do título de Mestre em Física.

Aprovada em: 17/12/2019.

BANCA EXAMINADORA

_____

Prof. José Wellington Rocha Tabosa
Orientador
Universidade Federal de Pernambuco

_____

Prof. Daniel Felinto Pires Barbosa
Examinador Interno
Universidade Federal de Pernambuco

_____

Prof. Thierry Marcelino Passerat de Silans
Examinador Externo
Universidade Federal da Paraíba

AGRADECIMENTOS

Primeiramente, gostaria de agradecer à minha família. Aos meus pais, Antonieta e Joaquim; por terem feito da educação a prioridade de nossa casa, pelo exemplo de caráter e por nunca terem me desencorajado de perseguir meus sonhos. A Jaime, por ter sido um irmão mais velho de verdade, me corrigindo quando eu estava errado e servindo como exemplo para minha vida pessoal e profissional. A Danielle e Izabelle, pela cumplicidade e companhia nos momentos mais difíceis e também nos mais divertidos. Aos meus avôs e minhas avós, por terem contribuído de forma direta e indireta para o meu desenvolvimento profissional. A irmãos, primos, tios e sobrinhos que me apoiaram e torceram para o sucesso deste trabalho.

Agradeço ao meu orientador, professor Tabosa. Sua dedicação, entusiasmo e seriedade servem de inspiração para os mais jovens. Agradeço também por ter me feito perceber a beleza da física experimental ainda durante o ciclo básico da graduação.

Aos professores, funcionários e amigos que fiz no Colégio Rosa Gattorno durante os 14 anos em que o frequentei. Lá me foram ensinados valores e conhecimento imprescindíveis para a continuidade de minha formação, além de ter feito amigos para toda a vida.

A todos os professores e funcionários que compõem o Departamento de Física da UFPE. Em especial: Paulo Campos, Leonardo Menezes, Mauro Copelli, Arkady Shanenko, Lúcio Acioli, Clécio Clemente, Alexsandra Melo e Daniel (da oficina eletrônica).

Aos membros da banca examinadora, pelas correções e sugestões que foram fundamentais para o desenvolvimento desta dissertação.

Aos amigos que fiz durante esses quase 6 anos de convivência no DF e que fizeram com que manhãs, tardes, noites, fins de semana e feriados de trabalho árduo fossem também divertidos e até inesquecíveis. Em especial: José, Diego (Guet), Mariana, Larissa, Juan, Wellington, Eriton, Alice, Polly, Leandro, Matteus e Alexandre.

A Jesús, Marcia e Allan, por terem me ensinado física, história, eletrônica, entre tantas outras coisas. E também pela amizade, que resultou em memoráveis pausas para cafés e conversas. Não consigo imaginar melhores colegas de laboratório.

À família que eu escolhi: minha esposa Nathália e meu filho Benjamin. Nathália por sua paciência, carinho, amor e apoio nos momentos mais difíceis. E Benjamin, por me fazer sorrir em todos os dias da duração deste mestrado, me mostrando o quanto a vida ainda é bela.

Por fim, agradeço ao povo brasileiro que por meio do CNPq, da CAPES e da FACEPE, fez com que este trabalho fosse possível.

ABSTRACT

Recoil-induced resonances (RIR) can be detected in experiments involving light-atom interaction where atomic external degrees of freedom play an important role. In pump-probe experiments the recoil of atoms due to absorption and emission of radiation is responsible for the amplification and attenuation of the probe beam under certain circumstances, resulting in a disperse and narrow (of the order of 10 kHz) feature in the spectrum of the probe beam. Backward four-wave mixing (BFWM) signals, via recoil-induced resonances, using cold atoms as nonlinear medium were also extensively studied during the past years. In this work it will be presented a systematic study of forward four-wave mixing (FFWM) via RIR. It will be also presented a simple theoretical model that allowed us to predict the lineshapes of the observed signals and to better understand the phenomenon studied. The model is also compared with results that are already known in order to verify its validity and predict the possibility of measure the velocity distribution of the atomic cloud in a future experiment.

Keywords: Recoil-induced resonances. Magneto-optical trap. Four-wave mixing. Atomic physics.

RESUMO

Ressonâncias induzidas por recuo (RIR) podem ser detectadas em experimentos envolvendo a interação de átomos com luz em situações em que graus de liberdade externos dos átomos desempenham papel fundamental. Em experimentos "pump-probe" o recuo de átomos devido à absorção e emissão de radiação é responsável pela amplificação e atenuação do feixe da sonda sob certas circunstâncias, resultando em um espectro de transmissão do feixe de sonda dispersivo e estreito (da ordem de 10 kHz). Sinais de mistura de quatro ondas para trás (BFWM), através de ressonâncias induzidas por recuo, usando átomos frios como meio não linear foram extensivamente estudados nos últimos anos. Neste trabalho, será apresentado um estudo sistemático da mistura de quatro ondas para frente (FFWM) via RIR. Também será apresentado um modelo teórico simples que nos permitiu prever as formas de linhas dos sinais observados e entender melhor o fenômeno estudado. O modelo também é comparado com resultados já conhecidos, a fim de verificar sua validade e prever a possibilidade de medir a distribuição de velocidade da nuvem atômica em um experimento futuro.

Palavras-chaves: Ressonâncias induzidas por recuo. Armadilha magneto-óptica. Mistura de quatro ondas. Física atômica.

LIST OF FIGURES

SUMMARY

1 INTRODUCTION

The quest for cooling down and trapping atoms, simultaneously, was one of the most thrilling scientific activities of the twentieth century. Its achievement was possible due to the work of many notable scientists, as for example: Claude Cohen-Tannoudji, Steven Chu and William D. Phillips. They shared the Nobel prize in Physics of 1997, for the development of methods to cool and trap atoms with laser light.

Moreover, a large number of further scientific achievements would not have been possible without these methods. The most remarkable is the realization of Bose-Einstein condensates [1, 2], that also defined the Nobel prize winners of 2001. But, the possibility of performing high precision experiments to investigate light-matter interaction, by spectroscopy, in an ensemble of cold atoms also led to many important developments in atomic, molecular and optical Physics.

Since the invention of laser by Maiman [3], spectroscopic techniques have been used to study physical properties of a variety of systems, from biological tissues to stars and galaxies. Atomic vapours have also been an important platform to perform coherent spectroscopy, and the development of magneto-optical traps (MOTs) [4] created the possibility of studying the structure and properties of atomic systems at low temperatures, and consequently low velocities, therefore eliminating Doppler broadening.

If the atoms are sufficiently cold, transitions between their momentum states can become important in the light-atom interaction. The recoil of atoms that are excited by the laser fields can lead to a redistribution of photons from one field to the other, resulting in the observation of recoil-induced resonances (RIR). The observation of this kind of ultranarrow resonance [5] was done just two years after its theoretical prediction [6].

Exploring the nonlinear effects in the atomic ensemble, observation of four-wave mixing signals associated with RIR could be performed, and recently it was related to the storage and multiplex of optical information [7], for example.

The main objective of this dissertation work is the observation and characterization of forward four-wave mixing (FFWM) via RIR. Four-wave mixing signals are a result of the interaction of light fields with a medium that has a nonlinear behaviour, and the observation of such signal via RIR in FFWM geometry has not been reported before in literature. In the experimental conditions of this work, the atoms can be simply treated as two-level systems with respect to their internal structure.

The study of multimode quantum correlations between FFWM signal and the probe's transmission is a possible application of the results presented here, since it was

studied before in a similar experimental configuration not related to RIR [8].

This dissertation is an experimental and theoretical study of forward four-wave mixing via recoil-induced resonances and it is divided into three chapters, as follows:

In chapter 1, the necessary physical fundamental concepts for the understanding of the atomic structure of ^{133}Cs are introduced. Furthermore, the forces acting in cesium atoms trapped in MOTs will be quantitatively and qualitatively explained. Although the explanation is done specifically for the case of cesium, the results obtained in this chapter could be extended for all alkaline atoms. Nonlinear effects that arise from light-matter interactions are briefly described, with emphasis on the generation of forward four-wave mixing. To finish the chapter, a theoretical description of the interaction between a three-level system and two classical electromagnetic fields will be done, the results will be used in chapter 3 to theoretically describe the experimental results. The chapter is not intended to be complete, hence some concepts of quantum mechanics are used without their demonstration, and a reader interested in a detailed explanation of such concepts can find it in references [12, 13].

The first section of Chapter 2 is dedicated to explain how recoil-induced resonances appear in pump-probe spectroscopy of cold atoms and why Raman processes between atomic external degrees of freedom lead to the amplification or attenuation of a probe beam in such experimental configuration. It is also calculated the effect of atomic recoil after an absorption-emission process in the external atomic energy and momentum, by simply assuming energy and momentum conservation in the light-atom system. Also, the generation of forward four-wave mixing by the incidence of two light fields in the atomic cloud is introduced, either by an usual four-wave mixing process or alternatively as a Bragg's diffraction of one of the beams in a grating of atomic density created by the interference between the two incident fields.

Additionally, the experiment is also described starting from MOT setup; along with an outline of the adopted procedures to properly measure the RIR spectrum in the transmission of the probe beam and the FFWM signal, including a general description of the experimental setup with the complete optical path of the laser beams and the time sequence of the experiment. To finish the chapter the obtained spectra are shown, as well as the dependence of the FFWM signal with respect to the pump's intensity.

In Chapter 3 the calculations performed in chapter 1 are used, considering the experimental conditions described in chapter 2, to theoretically reproduce the RIR and the FFWM spectra. The complete set of equations that represents the system is not solved; but the development of a simple and reasonable model is portrayed, together with its limitations. Theoretical results are shown and compared with the experimental ones. A comparison between results already known in the literature [32] and the results obtained from the model is performed in order to speculate the possibility of using the FFWM

signal as a method to measure the velocity distribution or the temperature of cold atoms.

Finally, the dissertation's conclusion is presented, in conjunction with some possible applications to the measured signal.

2 THEORETICAL CONCEPT

The aim of this chapter is to briefly develop the main ideas that led to various recent progresses in atomic physics. Nowadays, laser cooling and trapping of atoms and molecules are widely used in different kinds of experiments and their results are playing an important role in the advance of various areas of Physics, like: quantum optics [9], quantum information [10] and quantum simulations [11]. However, this dissertation is attained to the case of magneto-optical traps used to cool and trap neutral alkaline atoms. At first, it will be introduced the forces acting on atomic systems that made magneto-optical traps (MOT) [4] possible. Though recently MOTs were improved to trap atoms that are not hydrogen-like (alkalis), this text is focused on cesium atoms.

Secondly, it will be discussed the topics on nonlinear optics that are important to the understanding of four-wave mixing processes. The main original result of this dissertation is the observation and characterization of forward four-wave mixing via recoil-induced resonances (RIR).

Then, the development of a theory for the interaction of two electromagnetic fields with a nondegenerate three-level Λ system is presented.

2.1 MAGNETO-OPTICAL TRAP

The first important step in the counterintuitive achievement of laser cooling of neutral atoms was the proposition that low-density gases could be cooled by radiation pressure, made by Hänsch and Schalow [**?**]. The first experimental demonstration of laser cooling of atoms, deceleration of an atomic beam, by radiation pressure occurred 6 years later [15].

In the subsequent years, a huge development in the cooling and trapping of atomic beams took place, either using light or a combination of light and magnetic field. After the achievement of optical molasses, consisting of atoms cooled by three pairs of counterpropagating laser beams, the development of a magneto-optical trap making use of the hyperfine structure of the atoms and its magnetic sublevels was indispensable to the later progresses in atomic physics.

2.1.1 Atomic structure of Cesium-133

Alkali metals (alkalis) are all the elements of the periodic table that belong to its group 1. These elements are similar to each other with respect to their chemical properties, due to the fact that all of them have only one unpaired valence electron. One of the consequences of this structure is that it is needed less energy to put the valence electron in a higher sub-shell (excite the atom), compared to remove an electron from a closed sub-shell.

The possibility of easy excitation of the alkalis and the simplicity of making assumptions to theoretically analyze them, due to their similarity to hydrogen, made them (together with the hydrogen itself) natural candidates to experiments in atomic physics. For example, the first MOT was achieved using Na atoms. In this work the experiments were performed in a cloud of ^{133}Cs atoms, therefore the fundamental relevant properties of this isotope will be introduced.

The electronic structure of ^{133}Cs in the ground state is given by

$$1s^2 2s^2 2p^6 3s^2 3p^6 3d^{10} 4s^2 4p^6 4d^{10} 5s^2 5p^6 6s. \tag{2.1}$$

The number in front of each letter represents the principal quantum number (n), n = 1, 2, 3..., they are the numbers that determines the electron shell. The latin letters indicate the azimuthal quantum number (L), also known as angular momentum quantum number, their values are s = 0, p = 1, d = 2, f = 3, g = 4, etc. L determines the subshells of the atom. The intrinsic angular momentum of the electron is represented by the quantum number S = 1/2, it is called spin quantum number. The secondary spin quantum number (m_S) is also important and for the electron it can assume the values $\pm\frac{1}{2}$. The magnetic quantum numbers (m_L) can assume all integer values between -L and L. Together with n and L, m_L defines the electron's orbital, each orbital can contain up to 2 electrons and in order to satisfy Pauli's exclusion principle they have different m_S values.

As for the ^{133}Cs case there is only one valence electron, one can imagine that the core of the atom (nucleus + inner shell) orbits the electron. From this point of view the electron is subjected to an apparent magnetic field, because of the positive charge of the nucleus. The interaction between the effective magnetic field due to the orbit of the electron and its magnetic momentum, that is proportional to its spin angular momentum, results in an energy shift described by the Hamiltonian

$$\hat{H}_{LS} = A\vec{L} \cdot \vec{S}, \tag{2.2}$$

$A = \frac{(g_S - 1)\hbar^2}{m_e^2 c^2 r} \frac{\partial V}{\partial r}$, where g_S is the g-factor of the electron, m_e is the mass of the electron and V is the potential at which the valence electron is subjected. In order to compute the energy shift due to this coupling one should calculate the expected value of this expression,

using the Thomas precession factor and assuming the central field approximation (the procedure is more accurately described in [16]). The resulting energy shifts are given by

$$E_{LS} = A\frac{e^2}{8\pi\epsilon_0 n a_0 L(L+\frac{1}{2})(L+1)}(J(J+1) - L(L+1) - S(S+1)), \tag{2.3}$$

where a_0 is the Bohr radius and ϵ_0 is the vacuum permittivity. For electrons, J assumes the values $|\mathrm{L} \pm \frac{1}{2}|$, for each value of L. It can be seen in the electronic structure of the ^{133}Cs that the ground state ($L = 0$) can only assume one value of J, and the excited state ($6p$) can have $\mathrm{J} = \frac{1}{2}$ or $\mathrm{J} = \frac{3}{2}$. This gives rise to the fine structure of the atom and consequently the possibility of two different transitions. In this work the transition between the fine structure levels $6S_{\frac{1}{2}}$ and $6P_{\frac{3}{2}}$, known as the D_2 line of Cesium, was used.

The nucleus of the atom also has spin, described by the nuclear angular momentum quantum number (I), so a phenomenon similar to the previously explained can occur. The interaction of the nuclear magnetic moment and the magnetic field caused by the electron's motion gives rise to the hyperfine interaction. For the case of $L = 0$, the Hamiltonian of this coupling can be written as

$$\hat{H}_{HF} = B\vec{I}\cdot\vec{J}, \tag{2.4}$$

$B = \frac{2Z^3}{3\pi a_0^3 n^3}\mu_0\mu_N g_S \mu_B g_I$, where μ_0 is the vacuum permeability, μ_B is the Bohr magneton, g_I is the nuclear g-factor and μ_N is the nuclear magneton. Calculation of the expected value of the Hamiltonian, making use of the appropriate basis, results in

$$E_{HF} = \frac{B}{2}(F(F+1) - I(I+1) - J(J+1)). \tag{2.5}$$

F is the quantum number associated with the total angular momentum of the atom. It can assume values in the set

$$F = |J-I|, |J-I+1|, ..., J+I-1, J+I. \tag{2.6}$$

For the case of $L \neq 0$, for the purposes of this dissertation, the same Hamiltonian can be considered and also the expression of the energy shift remains the same.

Each hyperfine level is also 2(F+1) degenerated due to the magnetic sublevels. The magnetic sublevels are represented by the quantum number m_F that can assume the values

$$m_F = -F, -F+1, ...F-1, F. \tag{2.7}$$

It is also important to remember the selection rules that the possible transitions have to obbey

$$\Delta F = 0, \pm 1, \tag{2.8}$$

$$\Delta m_F = 0, \pm 1. \tag{2.9}$$

Figure 1: Hyperfine structure of the D_2 line of ^{133}Cs.

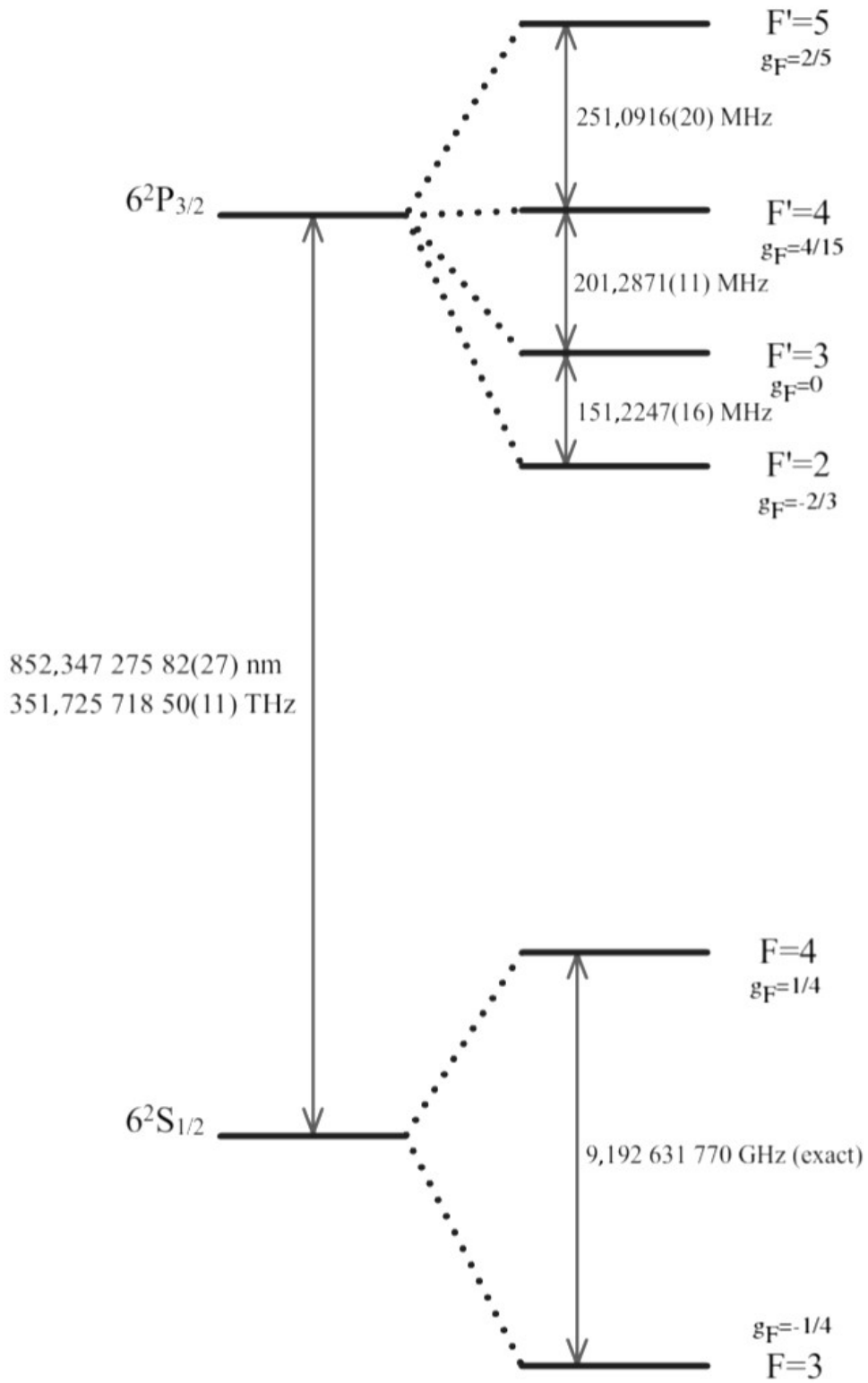

Source: Modified from [17].

In figure 1 the hyperfine structure of the D_2 line of ^{133}Cs is represented. It can be seen that as its nuclear spin is $\frac{7}{2}$, the quantum number F can assume the values $F = \{3, 4\}$ for the ground state and $F' = \{2, 3, 4, 5\}$ for the excited state.

2.1.2 Interaction between light and two-level systems

For the purposes of this dissertation the atoms will be considered as quantum objects and the light fields will be treated as classical electromagnetic fields. At this time the theory of the interaction of a two-level system with a classical electromagnetic wave will be developed. The field at this point will be described as

$$\vec{E}(\vec{r},t) = \vec{E_0}(\vec{r})(e^{i(\omega t - \vec{k}\cdot\vec{r})} + e^{-i(\omega t - \vec{k}\cdot\vec{r})}). \tag{2.10}$$

The Hamiltonian of the system is given by

$$\hat{H} = \hat{H}_a + \hat{V}_{al}, \tag{2.11}$$

$\hat{H}_a$ is the two-level atom's hamiltonian, including the internal and external degrees of freedom, and $\hat{V}_{al}$ is the representation of the interaction between the atom and the light field, in the electric dipole approximation. The interaction between the atom and the field is represented in figure 2.

$$\hat{H}_a = \frac{\hat{P}^2}{2m} + \hbar\omega_0|e\rangle\langle e|, \tag{2.12}$$

$$\hat{V}_{al} = -(\sum_{i=g,e}|i\rangle\langle i|)\hat{d}\cdot\vec{E}(\vec{r},t)(\sum_{j=g,e}|j\rangle\langle j|), \tag{2.13}$$

where $\hat{d}$ is the atomic dipole moment. It is induced in the atoms when they interact with the laser field, in the same direction of the field.

The time that is necessary to the internal dynamics of the atom to reach a steady state is much less than the time necessary to the external variables to be changed. This allows us to neglect the dynamics of the internal state assuming that it is in steady state, while describing the dynamics of the external states. More on this consideration and on the following calculations can be found in [20].

Defining the Rabi frequency as

$$\Omega(\vec{r}) = -\langle e|\frac{\hat{d}\cdot\vec{E}_0}{\hbar}|g\rangle, \tag{2.14}$$

the interaction between atom and light takes the form

$$\hat{V}_{al} = \hbar(e^{i(\omega t - \vec{k}\cdot\vec{r})} + e^{-i(\omega t - \vec{k}\cdot\vec{r})})\Omega(\vec{r})(|g\rangle\langle e| + |e\rangle\langle g|). \tag{2.15}$$

Figure 2: Interaction of a two-level system and one field.

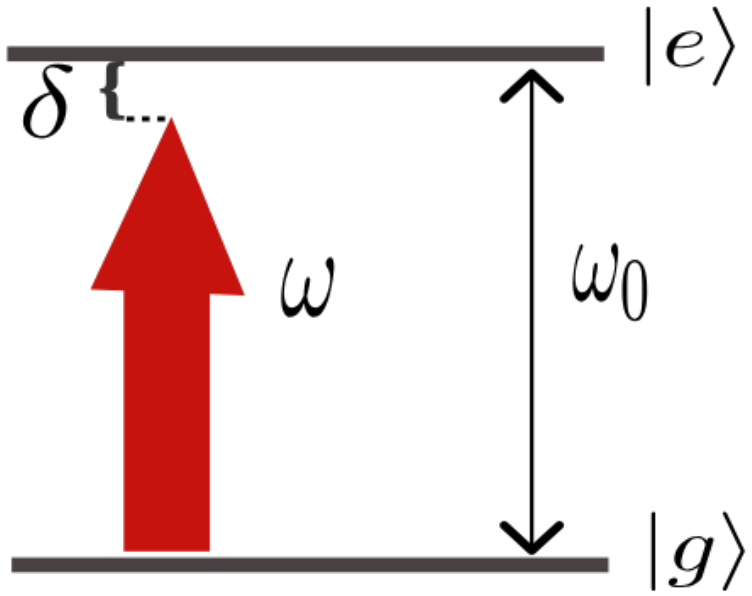

Source: The author (2019).

The mean force exerted on the atom is

$$\langle \vec{F} \rangle = \frac{\mathrm{d}\langle \hat{P} \rangle}{\mathrm{d}t}. \tag{2.16}$$

From the Liouville-von Neumman equation, the mean force can be written as

$$\langle \vec{F} \rangle = \frac{i}{\hbar} \langle \left[\hat{H}, \hat{P} \right] \rangle, \tag{2.17}$$

the only term of the hamiltonian that does not commute with $\hat{P}$ is $\hat{V}_{al}$, resulting in

$$\left[\hat{H}, \hat{P} \right] = i\hbar \vec{\nabla} \hat{V}_{al} \tag{2.18}$$

From 2.18 and 2.17

$$\langle \vec{F} \rangle = -\langle \vec{\nabla} \hat{V}_{al} \rangle. \tag{2.19}$$

Also, the mean value of a quantum operator can be calculated by the expression

$$\langle \hat{A} \rangle = \mathrm{Tr}\left(\hat{\rho} \hat{A} \right), \tag{2.20}$$

where $\hat{\rho}$ is the density operator. Finally, from 2.16, 2.19 and 2.20 we find that

$$\langle \vec{F} \rangle = -\mathrm{Tr}\left(\hat{\rho} \vec{\nabla} \hat{V}_{al} \right). \tag{2.21}$$

So, the average force acting on a two-level atom interacting with a classical electromagnetic field can be expressed in terms of the Rabi frequency, the phase of the field and the off-diagonal terms of the density operator as below

$$\langle \vec{F} \rangle = 2\hbar((\cos(\omega t - \vec{k} \cdot \vec{r}) \vec{\nabla} \Omega(\vec{r})) + \sin(\omega t - \vec{k} \cdot \vec{r}) \Omega(\vec{r}) \vec{\nabla}(\vec{k} \cdot \vec{r}))(\rho_{ge} + \rho_{ge}^*). \tag{2.22}$$

Now, to obtain ρ_{ge} (and ρ^*_{ge}) we should solve the optical Bloch equations (OBE) of the system, that are derived from the Liouville-von Neumman equation explicited below

$$i\hbar\frac{\mathrm{d}\hat{\rho}}{\mathrm{d}t} = \left[\hat{H}, \hat{\rho}\right]. \tag{2.23}$$

Developing 2.23 and using the properties $\rho_{ge} = \rho^*_{eg}$ and $\rho_{gg} + \rho_{ee} = 1$, we find

$$\dot{\rho}_{gg} = -i(\rho^*_{ge} - \rho_{ge})\Omega(\vec{r})(e^{i(\omega t - \vec{k}\cdot\vec{r})} + e^{-i(\omega t - \vec{k}\cdot\vec{r})}), \tag{2.24}$$

$$\dot{\rho}_{ee} = -i(\rho_{ge} - \rho^*_{ge})\Omega(\vec{r})(e^{i(\omega t - \vec{k}\cdot\vec{r})} + e^{-i(\omega t - \vec{k}\cdot\vec{r})}), \tag{2.25}$$

$$\dot{\rho}_{ge} = -i(\rho_{ee} - \rho_{gg})\Omega(\vec{r})(e^{i(\omega t - \vec{k}\cdot\vec{r})} + e^{-i(\omega t - \vec{k}\cdot\vec{r})}) + i\rho_{ge}\omega_0, \tag{2.26}$$

$$\dot{\rho}^*_{ge} = -i(\rho_{gg} - \rho_{ee})\Omega(\vec{r})(e^{i(\omega t - \vec{k}\cdot\vec{r})} + e^{-i(\omega t - \vec{k}\cdot\vec{r})}) - i\rho^*_{ge}\omega_0. \tag{2.27}$$

In $\hat{V}_{al}$ there will be terms oscillating with frequencies $|\omega_0 \pm \omega|$, since we assume that the dipole operator oscillates with frequency ω_0. It is reasonable to neglect the terms that oscillate with frequency $|\omega_0 + \omega|$, because the sum of the frequencies is much higher than their difference and the time of oscillation of the fields is negligible compared to the response time of the detectors used in the experiment. This approximation is known as rotating-wave approximation (RWA).

To facilitate the process of solving the equations, we also assume that in the stationary regime the coherences should oscillate with the frequency of the relevant field, resulting in $\sigma_{ge} = \rho_{ge}e^{-i(\omega t - \vec{k}\cdot\vec{r})}$, $\sigma_{ii} = \rho_{ii}$ with i = e, g.

Introducing terms related to spontaneous emission, where Γ is the decay rate of the excited state, results in the OBE of the system

$$\dot{\sigma}_{gg} = -i(\sigma^*_{ge} - \sigma_{ge})\Omega(\vec{r}) + \Gamma\sigma_{ee}, \tag{2.28}$$

$$\dot{\sigma}_{ee} = -i(\sigma_{ge} - \sigma^*_{ge})\Omega(\vec{r}) - \Gamma\sigma_{ee}, \tag{2.29}$$

$$\dot{\sigma}_{ge} = -i(\sigma_{ee} - \sigma_{gg})\Omega(\vec{r}) - (-i\omega_0 + \frac{\Gamma}{2} + i\omega)\sigma_{ge}. \tag{2.30}$$

Defining $\delta = \omega - \omega_0$ and assuming that the system is at a stationary state ($\dot{\sigma}_{ij} = 0$, with i, j = e, g) we find that

$$0 = -i(\sigma^*_{ge} - \sigma_{ge})\Omega(\vec{r}) + \Gamma\sigma_{ee}, \tag{2.31}$$

$$0 = -i(\sigma_{ge} - \sigma^*_{ge})\Omega(\vec{r}) - \Gamma\sigma_{ee}, \tag{2.32}$$

$$0 = -i(\sigma_{ee} - \sigma_{gg})\Omega(\vec{r}) - (i\delta + \frac{\Gamma}{2})\sigma_{ge}. \tag{2.33}$$

Equations 2.31 and 2.32 are the same and have as result

$$\sigma_{ee} = \frac{i(\sigma^*_{ge} - \sigma_{ge})\Omega(\vec{r})}{\Gamma}. \tag{2.34}$$

Inserting 2.34 and $\sigma_{gg} + \sigma_{ee} = 1$ in 2.33 to finally solve for σ_{ge}, we obtain

$$\sigma_{ge} = \frac{\Omega(\vec{r})(\delta + i\frac{\Gamma}{2})}{\delta^2 + \frac{\Gamma^2}{4} + 2\Omega^2(\vec{r})}. \tag{2.35}$$

Figure 3: One atom interacting with two counterpropagating laser beams.

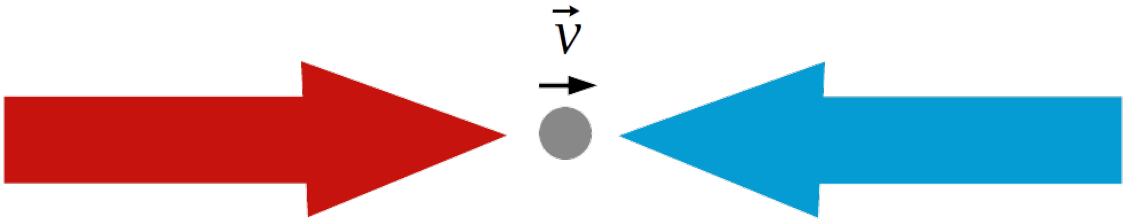

Source: The author (2019).

Now, from 2.35, $\sigma_{ge} = \rho_{ge}e^{-i(\omega t - \vec{k}\cdot\vec{r})}$ and 2.22 we can find an expression for the force acting in an atom at $\vec{r} = 0$, after averaging for one optical period

$$\langle \vec{F} \rangle = -\frac{\hbar\Omega\left[2\delta\vec{\nabla}\Omega - \Gamma\Omega\vec{\nabla}(\vec{k}\cdot\vec{r})\right]}{\delta^2 + \frac{\Gamma^2}{4} + 2\Omega^2}. \tag{2.36}$$

The first term can be recognized as the dipole force, which is conservative with a potential given by

$$U_{dip} = \hbar\delta ln\Big(1 + \frac{2\Omega^2}{\delta^2 + \frac{\Gamma^2}{4}}\Big), \tag{2.37}$$

and the second term is the force related to radiation pressure, that is dissipative.

2.1.3 Cooling neutral atoms

Before introducing the magneto-optical trap itself, it is important to discuss a preliminary step in its procedure. The optical molasses technique [24] is a technique to cool atoms to very low temperatures. It consists in the incidence of 3 pairs of counterpropagating laser beams, red-detuned from the atomic resonance, in a gas of atoms.

In view of a simple explanation we will consider an atom that has only one transition that effectively couples with the fields (for our considerations this is a 'two-level atom'), moving in just one axis ($\hat{z}$) with a small velocity $\vec{v}$ in the same direction of one of the beams ($+\hat{z}$), like depicted in the figure 3.

As a result of the consideration that the spatial dependence of the field is nearly constant in the region of interaction with the atoms, we assume that $\vec{\nabla}\Omega(\vec{r}) \approx 0$. Then, the first term in 2.36 vanishes. As the atom is moving, δ is shifted by $\vec{k}\cdot\vec{v}$, by the Doppler effect. The effect of this shift is shown in Fig.4. It is clear that the detuning of the transition with the counterpropagating beam becomes closer to resonance, i.e. $\delta' = \delta + kv$, while the

Figure 4: Interaction of a two-level system and two electromagnetic fields, that propagate in the same orientation, but opposite sense. The system (atom) is moving in the same sense of the red beam.

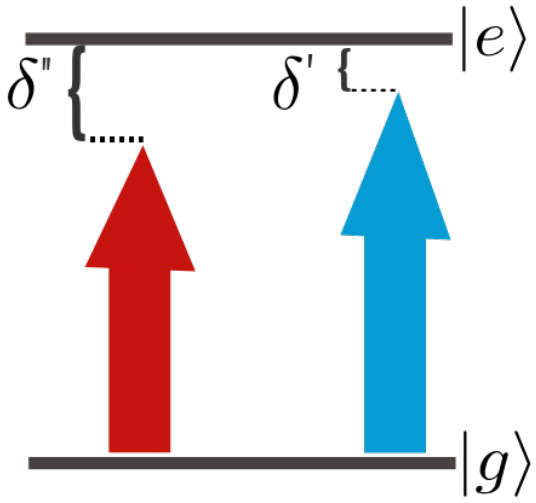

Source: The author (2019).

detuning with the copropagating beam is increased, i.e. $\delta'' = \delta - kv$. Then, it is more probable that the atom will be excited by the counterpropagating beam.

Introducing this shift in the remaining expression of the force and expanding it until the first order as a Taylor series around $|v| = 0$ results in

$$\vec{F} = -\alpha\vec{v}, \tag{2.38}$$

where

$$\alpha = \frac{4|\delta|\hbar\Omega^2 k^2\Gamma}{(\delta^2 + \frac{\Gamma^2}{4} + 2\Omega^2)^2}.$$

This is a velocity dependent force, responsible for the cooling of atoms. But, as this force is only velocity-dependent, the atoms will not be confined by this force and can leave the region of interaction with the beams. Then, atoms that are subject to this force are cold but not trapped.

2.1.4 Trapping neutral atoms

To achieve a MOT, the radiation pressure force needs to be position dependent. Jean Dalibard suggested the addition of a spatial gradient of a quadrupole magnetic field [4]. This magnetic field, generated by two coils in the anti-Helmholtz configuration, combined with three pairs of counterpropagating laser beams of circular and opposed polarizations would produce the force necessary to cool and trap the atoms.

Figure 5: Configuration of a 3-fold degenerate excited state and a nondegenerate ground state interacting with two counterpropagating circularly polarized beams, in the presence of a magnetic field that varies linearly with respect to the position.

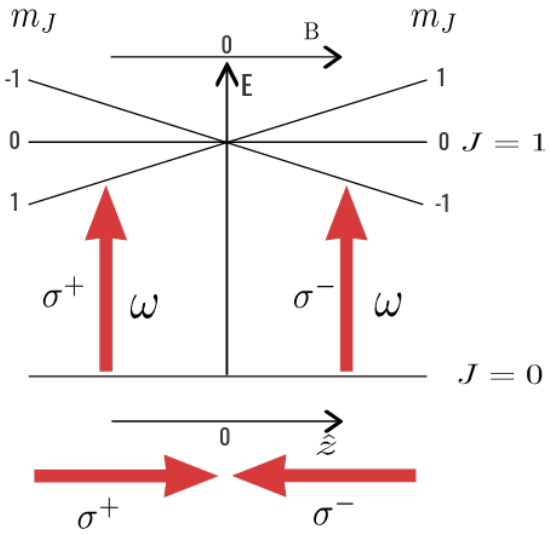

Source: The author (2019).

Similarly to what was done in the previous section, we will consider an atom moving in just one dimension ($\hat{z}$). For simplicity, it will be assumed that the relevant transition is from a level J = 0 to J' = 1. The magnetic field depends linearly on the position, so the detuning becomes $\delta = \omega - \omega_0 - \vec{k} \cdot \vec{v} \pm \gamma_F bz$. b is the gradient of the magnetic field, given by $B(z) = bz\hat{z}$, $\gamma_F = \frac{g_F \mu_B}{\hbar}$, and g_J is the Landé factor of the excited state.

Thus, if the atom is localized in some point at the positive part of the z axis, it will be more likely to interact with the σ^- beam. If it is in the negative part of the axis, it will have more probability to be excited by the σ^+ beam. This can be seen in Fig.5. Another way to see the effect of the magnetic field is expanding 2.36 in a Taylor series considering the corrections related to the atom's velocity and the position dependent magnetic field. Assuming $|\vec{v}| \approx 0$ and $|\vec{z}| \approx 0$:

$$\vec{F} = -\alpha\vec{v} - \beta\vec{z}, \tag{2.39}$$

where

$$\beta = \frac{4|\delta|\gamma_J b\hbar\Omega^2 k^2 \Gamma}{(\delta^2 + \frac{\Gamma^2}{4} + 2\Omega^2)^2}, \tag{2.40}$$

and α is the same of 2.38.

Finally, we note that this system is clearly similar to a classical damped harmonic oscillator. Then, atoms that are subject to this forces will be cooled and trapped. An illustration of an operating MOT can be seen in figure 6.

Figure 6: Illustration of an operating MOT.

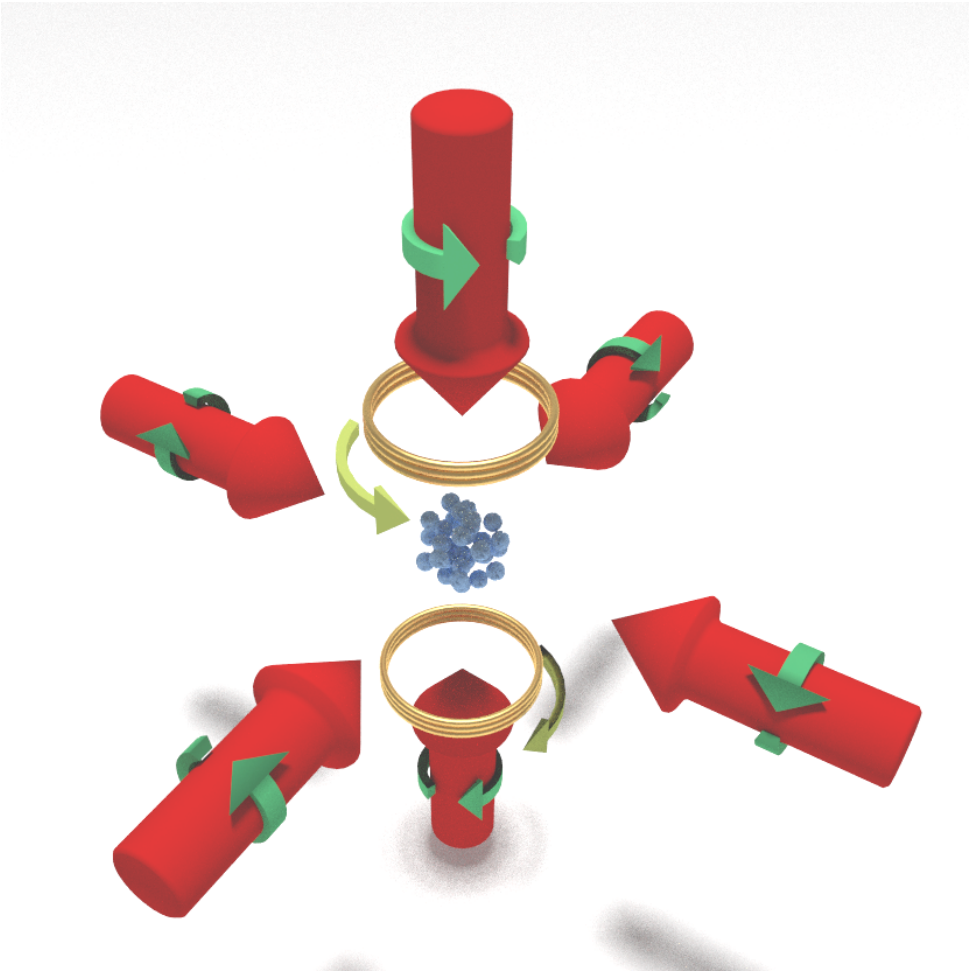

Source: Modified from [19].

2.1.5 Doppler limit

The Doppler cooling technique described above was very important to the achievement of gases at temperatures that were unreachable before its invention. But this method does not enable the cooling of atoms indefinitely. The limit temperature that can be achieved is known as Doppler limit.

The derivation of this limit for the case of only two counterpropagating beams (1D case) can be done considering the process of absorption from the field followed by spontaneous emission. The net effect of each of the mentioned processes is the changing in the momentum of the atom by $\hbar\vec{k}$. The frequency of the absorbed mode is given by $\omega_{abs} = \omega_0 + \omega_R$ and the frequency of the emitted mode is $\omega_{emt} = \omega_0 - \omega_R$, where $\hbar\omega_R$ is the recoil energy. Then, the field loses an average energy of $2\hbar\omega_R$ for each absorption-emission process.

The consideration of only two counterpropagating beams results in a total excitation

increase rate of $2\Gamma\sigma_{ee}$, where σ_{ee} is the population of the excited state. The population of the excited state can be calculated by just inserting 2.35 in 2.34. So, the average heating of the atoms is $4\Gamma\sigma_{ee}\hbar\omega_R$. Then

$$\Delta E_{heating} = \frac{4\hbar\Gamma\Omega^2\omega_R}{\delta^2 + \frac{\Gamma^2}{4} + 2\Omega^2}. \tag{2.41}$$

The rate of dissipation of energy in the molasses is $\Delta E_{dis} = -\alpha v^2$, where α is the same of 2.38 and v is the modulus of the velocity of the atom. This results in:

$$\Delta E_{dis} = \frac{4\hbar\Gamma\Omega^2 k^2 \delta v^2}{(\delta^2 + \frac{\Gamma^2}{4} + 2\Omega^2)^2}. \tag{2.42}$$

Thus under equilibrium condition, we should have $\Delta E_{dis} = \Delta E_{heating}$. Noting that $\omega_R = \frac{\hbar k^2}{2m}$, we obtain

$$v^2 = \frac{\hbar(\delta^2 + \frac{\Gamma^2}{4})}{2m\delta}. \tag{2.43}$$

From the equipartition theorem and considering $\Omega << \Gamma$, we have that $\frac{mv^2}{2} = \frac{k_B T}{2}$. Then

$$T = \frac{\hbar(\delta^2 + \frac{\Gamma^2}{4})}{2\delta k_B}. \tag{2.44}$$

This relation assumes a physical minimum value when $\delta = -\frac{\Gamma}{2}$, which defines the Doppler temperature as

$$T_D = \frac{\hbar\Gamma}{2k_B}. \tag{2.45}$$

For ^{133}Cs the value of the Doppler temperature is 125 μK.

2.2 TOPICS ON NONLINEAR OPTICS

It is known from classical electrodynamics that electromagnetic phenomena are described by the macroscopic Maxwell's equations, that in SI units are

$$\vec{\nabla} \cdot \vec{D} = \rho_f, \tag{2.46}$$

$$\vec{\nabla} \cdot \vec{B} = 0, \tag{2.47}$$

$$\vec{\nabla} \times \vec{E} = -\frac{\partial \vec{B}}{\partial t}, \tag{2.48}$$

$$\vec{\nabla} \times \vec{H} = \vec{J}_f + \frac{\partial \vec{D}}{\partial t}, \tag{2.49}$$

where $\vec{D} \equiv \epsilon_0 \vec{E} + \vec{P}$ is the electric displacement field, ρ_f is the density of free charges in the medium, $\vec{H} \equiv \frac{\vec{B}}{\mu_0} - \vec{M}$ is the analogous of $\vec{D}$ for the magnetic field, $\vec{J}_f$ is the density

of free currents in the medium, $\vec{P}$ is the polarization field and $\vec{M}$ is the magnetization field. For our purposes $\vec{M}$, ρ_f and $\vec{J}_f$ can be neglected.

Taking the curl of 2.48, using the relation $\vec{\nabla} \times \vec{\nabla} \times \vec{A} = \vec{\nabla}(\vec{\nabla} \cdot \vec{A}) - \nabla^2 \vec{A}$, and 2.46, result in

$$\nabla^2 \vec{E} = \mu_0 \frac{\partial \vec{\nabla} \times \vec{H}}{\partial t}. \tag{2.50}$$

Inserting 2.49 in 2.50, we find a wave equation

$$\nabla^2 \vec{E} = \epsilon_0 \mu_0 \frac{\partial^2 \vec{E}}{\partial t^2} + \mu_0 \frac{\partial^2 \vec{P}}{\partial t^2}. \tag{2.51}$$

A linear medium has a linear constitutive relation of the form

$$\vec{P} = \epsilon_0 \chi \vec{E}, \tag{2.52}$$

where χ is the electric susceptibility. But the general representation of the polarization takes into account higher order terms. The nonlinear expression for the polarization neglecting the tensorial nature of the electric susceptibility, i.e. considering that the medium is isotropic, is given by

$$P = \epsilon_0 [\chi^{(1)} E + \chi^{(2)} E^2 + \chi^{(3)} E^3 + ...]. \tag{2.53}$$

One can divide the polarization in two parts: linear and nonlinear. The linear part is given by 2.52, the nonlinear terms will be represented by P_{NL} and we can also define

$$\epsilon = \epsilon_0 (\chi^{(1)} + 1), \tag{2.54}$$

resulting in a wave equation for electromagnetic fields with the nonlinear polarization playing the role of a source for the generated fields

$$\nabla^2 \vec{E} - \epsilon \mu_0 \frac{\partial^2 \vec{E}}{\partial t^2} = \mu_0 \frac{\partial^2 \vec{P}_{NL}}{\partial t^2}. \tag{2.55}$$

2.2.1 Four-wave mixing

In an ensemble of cold ^{133}Cs the nonlinear susceptibilities of even orders, χ^{2n} where $n \in \mathbb{N}$, are zero due to the spatial-reverse symmetry of the ensemble. But the $\chi^{(3)}$ term plays an important role in this kind of medium, leading to the appearance of third-order nonlinear phenomena. For our purposes the nonlinear polarization, neglecting higher order terms, can be considered as just

$$P_{NL} = \epsilon_0 \chi^{(3)} E^3. \tag{2.56}$$

In the case of two fields propagating in the medium, the total electromagnetic field can be described as:

$$E = [E_1(\omega_1)e^{-i\vec{k_1}\cdot\vec{r}+i\omega_1 t} + E_2(\omega_2)e^{-i\vec{k_2}\cdot\vec{r}+i\omega_2 t} + c.c], \tag{2.57}$$

inserting 2.56 and 2.57 in 2.55 leads to the generation of fields propagating in different directions, one of these processes is known as four-wave mixing and it has been extensively studied in different systems, e.g. [22, 23]. The directions depend on the combination of the wavevectors of the fields. In this work we are interested in the generated field E_3 that is proportional to $E_2^{*2}E_1$ in the case of E_1 and E_2 nearly copropagating, called forward four-wave mixing field.

It can be shown that the efficiency of this four-wave mixing process is maximum when [21]:

$$\vec{k_3} = 2\vec{k_2} - \vec{k_1}, \tag{2.58}$$

where $\vec{k_3}$ is the wavevector of the generated field. This result is known as the phase-matching condition. When this condition is not fulfilled, the generation of a field can still occurs in some situations. In these cases the efficiency of the four-wave mixing process decreases with the wavevector mismatch, defined by:

$$\Delta\vec{k} = 2\vec{k_2} - \vec{k_1} - \vec{k_3}. \tag{2.59}$$

2.2.2 Absorption coefficient

In the interaction of a weak light field and an atomic ensemble, the field excites atoms and this effect results in a polarization that gives rise to an absorption of the field. This effect will be important in the next chapters, where the transmission of a probe field after passing through a cloud of cold atoms was measured and the spectrum of this signal was recorded. The gain and absorption coefficient of a field can be theoretically modeled by calculating the propagation of the field in the medium. For a field described as

$$\vec{E}(z,t) = \vec{E_0}(e^{i(\omega t - kz)} + c.c), \tag{2.60}$$

to find the absorption coefficient we should first remember that the propagation velocity of the field in a medium that is not magnetic is given by

$$v = \frac{1}{\sqrt{\mu_0\epsilon}}. \tag{2.61}$$

Inserting 2.54 in this expression, using the definition of the speed of light in vacuum, $c = \frac{1}{\sqrt{\mu_0\epsilon_0}}$, and assuming $\chi << 1$:

$$k = \frac{\omega}{v} \approx \frac{\omega}{c}(1 + \frac{1}{2}\chi). \tag{2.62}$$

χ is an imaginary quantity, so it can be written as

$$\chi = \chi_1 + i\chi_2, \tag{2.63}$$

where χ_1 is the real part and χ_2 the imaginary part of χ. Making use of 2.62 and 2.63 we find the expression for the electromagnetic field propagating through the medium:

$$\vec{E}(z,t) = \vec{E_0}(e^{i(\omega t - \frac{\omega}{c}(1+\frac{1}{2}\chi_1)z) - \frac{\omega}{2c}\chi_2 z} + c.c). \tag{2.64}$$

It is clear that the resulting field is attenuated by a factor of $e^{-\frac{\alpha z}{2}}$, where $\alpha = \frac{\omega}{c}\chi_2$ is the absorption coefficient.

There is a simple relation between the absorption coefficient derived and the coherence between the excited and the ground state. This relation will be calculated for the case of a field that just couples with one transition (two-level atoms) and in the regime where 2.52 is satisfied.

The average of the linear polarization can be written as

$$P = N\langle\hat{d}\rangle, \tag{2.65}$$

where N is the number of atoms and $\langle\hat{d}\rangle$ is the mean value of the atomic dipole moment defined before.

Inserting 2.20 and 2.14 in 2.65 and 2.52 we find that

$$\chi = \frac{N|d_{ge}|^2\sigma_{ge}}{\Omega(z,t)\hbar\epsilon_0}. \tag{2.66}$$

It is also important to consider the generated field (four-wave mixing) in this case, since it is the main objective of this work. The equation 2.55 means that the generated field is proportional to the induced polarization, so the intensity of the field is proportional to the modulus squared of the polarization, that is proportional to χ, as can be seen in 2.66. Then

$$I \propto |\sigma_{ge}|^2, \tag{2.67}$$

where I is the intensity of the generated field. This result will be also used in the next chapters to predict the lineshape of the forward four-wave mixing signal via RIR.

2.3 INTERACTION OF TWO ELECTROMAGNETIC FIELDS WITH A NONDEGENERATE THREE-LEVEL Λ SYSTEM

In this section we will consider the interaction of two electromagnetic fields interacting with a nondegenerate 3-level system in a λ configuration, as shown in 7.

Figure 7: Interaction of a three-level system and two electromagnetic fields. Δ represents the detuning between the field E_2 and the transition $|a\rangle - |c\rangle$, Δ_0 is the frequency gap between $|a\rangle$ and $|b\rangle$ and $\Delta_R = \omega_1 - \omega_2 + \Delta_0$.

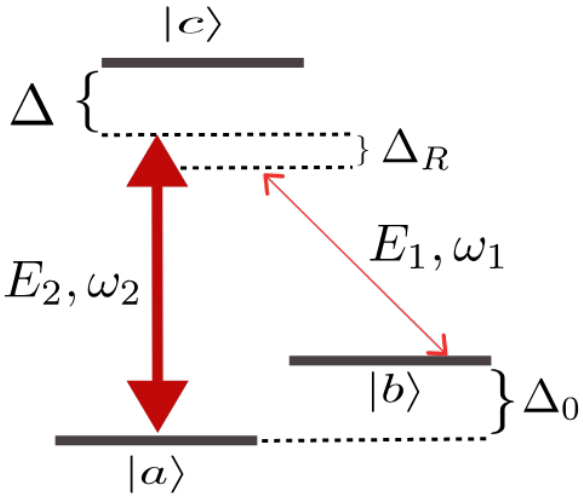

Source: The author (2019).

2.3.1 Hamiltonian

The system's Hamiltonian is given by:

$$\hat{H} = \hat{H}_0 + \hat{V}_{al}$$

$\hat{H}_0$ is the Hamiltonian of a three-level atom and $\hat{V}_{al}$ represents the interaction between the atom and the fields. Assuming as basis $\{|a\rangle, |b\rangle, |c\rangle\}$ and remembering that

$$\sum_i |i\rangle\langle i| = \hat{I} \qquad (i = a, b, c)\,, \tag{2.68}$$

we have

$$\hat{H}_0|i\rangle = E_i|i\rangle. \tag{2.69}$$

Then, applying 2.68 to right and left of $\hat{H}_0$ and making use of 2.69

$$\hat{H}_0 = -\hbar(\omega_a|a\rangle\langle a| + \omega_b|b\rangle\langle b| + \omega_c|c\rangle\langle c|). \tag{2.70}$$

The interaction's Hamiltonian is given by

$$\hat{V}_{al} = -(\sum_{i=a,b,c} |i\rangle\langle i|)\hat{d}\cdot\vec{E}(\vec{r},t)(\sum_{j=a,b,c} |j\rangle\langle j|).$$

Because of the parity of the position operator and $\hat{d} = e\hat{X}$, where e is the electron's charge and $\hat{X}$ is the position operator, we have that

$$\langle i|\hat{d}\cdot\vec{E}|i\rangle = 0. \tag{2.71}$$

The electromagnetic field can be written as

$$\vec{E}(t) = E_1 e^{-i\omega_1 t}\hat{z} + E_1 e^{i\omega_1 t}\hat{z} + E_2 e^{-i\omega_2 t}\hat{z} + E_2 e^{i\omega_2 t}\hat{z}.$$

So, we define the Rabi frequencies of the fields as

$$\Omega_1 = -\langle b|\frac{\hat{d}\cdot\vec{E}_1}{\hbar}|c\rangle, \qquad \Omega_2 = -\langle a|\frac{\hat{d}\cdot\vec{E}_2}{\hbar}|c\rangle, \tag{2.72}$$

where E_1 is proportional to $e^{-i\vec{k}_1\cdot\vec{r}}$ and E_2 proportional to $e^{-i\vec{k}_2\cdot\vec{r}}$. Assuming that $\vec{E}_1$ couples with the transition $|b\rangle$ - $|c\rangle$ and $\vec{E}_2$ field couples with the transition $|a\rangle$ - $|c\rangle$, which reasonably agrees with the experimental conditions, result in an the interaction Hamiltonian given by

$$\begin{aligned}\hat{V}_{al} = &-\hbar[\Omega_1(e^{-i\omega_1 t} + e^{i\omega_1 t})|b\rangle\langle c| + \Omega_1^*(e^{-i\omega_1 t} + e^{i\omega_1 t})|c\rangle\langle b| + \Omega_2(e^{-i\omega_2 t} + e^{i\omega_2 t})|a\rangle\langle c| + \\ &\Omega_2^*(e^{-i\omega_2 t} + e^{i\omega_2 t})|c\rangle\langle a|].\end{aligned}$$

Finally, the total Hamiltonian in the matrix form is

$$\hat{H} = -\hbar\begin{pmatrix} \omega_a & 0 & \Omega_2(e^{-i\omega_2 t} + e^{i\omega_2 t}) \\ 0 & \omega_b & \Omega_1(e^{-i\omega_1 t} + e^{i\omega_1 t}) \\ \Omega_2^*(e^{-i\omega_2 t} + e^{i\omega_2 t}) & \Omega_1^*(e^{-i\omega_1 t} + e^{i\omega_1 t}) & \omega_c \end{pmatrix}. \tag{2.73}$$

2.3.2 Bloch equations

The matrix representation of the density operator is

$$\hat{\rho} = \begin{pmatrix} \rho_{aa} & \rho_{ab} & \rho_{ac} \\ \rho_{ba} & \rho_{bb} & \rho_{bc} \\ \rho_{ca} & \rho_{cb} & \rho_{cc} \end{pmatrix}. \tag{2.74}$$

The time evolution of the density operator is given by 2.23. Developing it, with the Hamiltonian of the system given by 2.73, we obtain

$$\dot{\rho}_{aa} = i(e^{-i\omega_2 t} + e^{i\omega_2 t})(\Omega_2\rho_{ca} - \Omega_2^*\rho_{ac}), \tag{2.75}$$
$$\dot{\rho}_{bb} = i(e^{-i\omega_1 t} + e^{i\omega_1 t})(\Omega_1\rho_{cb} - \Omega_1^*\rho_{bc}), \tag{2.76}$$
$$\dot{\rho}_{cc} = i(e^{-i\omega_2 t} + e^{i\omega_2 t})(\Omega_2^*\rho_{ac} - \Omega_2\rho_{ca}) + i(e^{-i\omega_1 t} + e^{i\omega_1 t})(\Omega_1^*\rho_{bc} - \Omega_1\rho_{cb}), \tag{2.77}$$
$$\dot{\rho}_{ab} = i(\omega_a - \omega_b)\rho_{ab} + i\Omega_2(e^{-i\omega_2 t} + e^{i\omega_2 t})\rho_{cb} - i\Omega_1^*(e^{-i\omega_1 t} + e^{i\omega_1 t})\rho_{ac}, \tag{2.78}$$
$$\dot{\rho}_{ac} = i(\omega_a - \omega_c)\rho_{ac} + i\Omega_2(e^{-i\omega_2 t} + e^{i\omega_2 t})(\rho_{cc} - \rho_{aa}) - i\Omega_1(e^{-i\omega_1 t} + e^{i\omega_1 t})\rho_{ab}, \tag{2.79}$$
$$\dot{\rho}_{ba} = i(\omega_b - \omega_a)\rho_{ba} + i\Omega_1(e^{-i\omega_1 t} + e^{i\omega_1 t})\rho_{ca} - i\Omega_2^*(e^{-i\omega_2 t} + e^{i\omega_2 t})\rho_{bc}, \tag{2.80}$$
$$\dot{\rho}_{bc} = i(\omega_b - \omega_c)\rho_{bc} + i\Omega_1(e^{-i\omega_1 t} + e^{i\omega_1 t})(\rho_{cc} - \rho_{bb}) - i\Omega_2(e^{-i\omega_2 t} + e^{i\omega_2 t})\rho_{ab}, \tag{2.81}$$
$$\dot{\rho}_{ca} = i(\omega_c - \omega_a)\rho_{ca} + i\Omega_2^*(e^{-i\omega_2 t} + e^{i\omega_2 t})(\rho_{aa} - \rho_{cc}) + i\Omega_1^*(e^{-i\omega_1 t} + e^{i\omega_1 t})\rho_{ba}, \tag{2.82}$$
$$\dot{\rho}_{cb} = i(\omega_c - \omega_b)\rho_{cb} + i\Omega_2^*(e^{-i\omega_2 t} + e^{i\omega_2 t})\rho_{ab} + i\Omega_1^*(e^{-i\omega_1 t} + e^{i\omega_1 t})(\rho_{bb} - \rho_{cc}). \tag{2.83}$$

Introducing terms related to the relaxation of population and coherence and taking into account that $\rho_{ij} = \rho^*_{ji}$, we have to solve the equations:

$$\begin{aligned}\dot{\rho}_{cc} &= -(\gamma + \gamma_{ca} + \gamma_{cb})\rho_{cc} + (e^{-i\omega_2 t} + e^{i\omega_2 t})(\Omega^*_2\rho^*_{ca} - \Omega_2\rho_{ca}) \\ &\quad + i(e^{-i\omega_1 t} + e^{i\omega_1 t})(\Omega^*_1\rho^*_{cb} - \Omega_1\rho_{cb}),\end{aligned} \tag{2.84}$$

$$\dot{\rho}_{aa} = \gamma\rho^0_{aa} + \gamma_{ca}\rho_{cc} - \gamma\rho_{aa} + i(e^{-i\omega_2 t} + e^{i\omega_2 t})(\Omega_2\rho_{ca} - \Omega^*_2\rho^*_{ca}), \tag{2.85}$$

$$\dot{\rho}_{bb} = \gamma\rho^0_{bb} + \gamma_{cb}\rho_{cc} - \gamma\rho_{bb} + i(e^{-i\omega_1 t} + e^{i\omega_1 t})(\Omega_1\rho_{cb} - \Omega^*_1\rho^*_{cb}), \tag{2.86}$$

$$\begin{aligned}\dot{\rho}_{ca} &= -\frac{1}{2}(2\gamma + \gamma_{cb} + \gamma_{ca} - 2i\omega_{ca})\rho_{ca} + i\Omega^*_2(e^{-i\omega_2 t} + e^{i\omega_2 t})(\rho_{aa} - \rho_{cc}) \\ &\quad + i\Omega^*_1(e^{-i\omega_1 t} + e^{i\omega_1 t})\rho^*_{ab},\end{aligned} \tag{2.87}$$

$$\begin{aligned}\dot{\rho}_{cb} &= -\frac{1}{2}(2\gamma + \gamma_{cb} + \gamma_{ca} - 2i\omega_{cb})\rho_{cb} + i\Omega^*_2(e^{-i\omega_2 t} + e^{i\omega_2 t})\rho_{ab} \\ &\quad + i\Omega^*_1(e^{-i\omega_1 t} + e^{i\omega_1 t})(\rho_{bb} - \rho_{cc}),\end{aligned} \tag{2.88}$$

$$\dot{\rho}_{ab} = -(\gamma - i\omega_{ab})\rho_{ab} + i\Omega_2(e^{-i\omega_2 t} + e^{i\omega_2 t})\rho_{cb} - i\Omega^*_1(e^{-i\omega_1 t} + e^{i\omega_1 t})\rho^*_{ca}. \tag{2.89}$$

Where:

- -$\gamma\rho_{ii}$ are related to the loss of population of the system, since γ is the rate of which atoms leave or enter the region of interaction with the fields;
- terms with $\gamma_{cj}\rho_{cc}$, where j = $\{a, b\}$, represent the loss of population from $|c\rangle$ to $|a\rangle$ or $|b\rangle$;
- -$\gamma_{cj}\rho_{cj}$, with j = $\{a, b\}$ and -$\gamma\rho_{ij}$, for i $\neq$ j, represent the loss of coherence of the system;
- $\gamma\rho^0_{ii}$ are related to the gain in population of the states $|a\rangle$ and $|b\rangle$;
- $\omega_{ij} = \omega_i - \omega_j$.

Defining new variables as $\sigma_{ca} = \rho_{ca}e^{-i\omega_2 t}$, $\sigma_{cb} = \rho_{cb}e^{-i\omega_1 t}$, $\sigma_{ab} = \rho_{ab}e^{-i(\omega_1-\omega_2)t}$, $\sigma_{ii} = \rho_{ii}$; rearranging the terms and applying the rotating wave approximation (RWA), which means to assume that terms of frequencies | $\pm 2\omega_1$ | and | $\pm 2\omega_2$ | oscillate too fast and can be neglected, results in

$$\dot{\sigma}_{cc} = -(\gamma + \gamma_{ca} + \gamma_{cb})\sigma_{cc} + i(\Omega^*_2\sigma^*_{ca} - \Omega_2\sigma_{ca}) + i(\Omega^*_1\sigma^*_{cb} - \Omega_1\sigma_{cb}), \tag{2.90}$$

$$\dot{\sigma}_{aa} = \gamma\sigma^0_{aa} + \gamma_{ca}\sigma_{cc} - \gamma\sigma_{aa} + i(\Omega_2\sigma_{ca} - \Omega^*_2\sigma^*_{ca}), \tag{2.91}$$

$$\dot{\sigma}_{bb} = \gamma\sigma^0_{bb} + \gamma_{cb}\sigma_{cc} - \gamma\sigma_{bb} + i(\Omega_1\sigma_{cb} - \Omega^*_1\sigma^*_{cb}), \tag{2.92}$$

$$\dot{\sigma}_{ca} = -\frac{1}{2}(2\omega_2 + 2\gamma + \gamma_{cb} + \gamma_{ca} - 2i\omega_{ca})\sigma_{ca} + i\Omega^*_2(\sigma_{aa} - \sigma_{cc}) + i\Omega^*_1\sigma^*_{ab}, \tag{2.93}$$

$$\dot{\sigma}_{cb} = -\frac{1}{2}(2\omega_1 + 2\gamma + \gamma_{cb} + \gamma_{ca} - 2i\omega_{cb})\sigma_{cb} + i\Omega^*_2\sigma_{ab} + i\Omega^*_1(\sigma_{bb} - \sigma_{cc}), \tag{2.94}$$

$$\dot{\sigma}_{ab} = -(-i\omega_{21} + \gamma - i\omega_{ab})\sigma_{ab} + i\Omega_2\sigma_{cb} - i\Omega^*_1\sigma^*_{ca}. \tag{2.95}$$

$$\tag{2.96}$$

Defining

$$\Gamma_0 = \gamma_{cb} + \gamma_{ca}, \tag{2.97}$$

$$\delta = \omega_{12} = \omega_1 - \omega_2, \tag{2.98}$$

$$\beta_{cb} = -\gamma - \frac{\Gamma_0}{2} + i(\omega_{cb} - \omega_1), \tag{2.99}$$

$$\beta_{ca} = -\gamma - \frac{\Gamma_0}{2} + i(\omega_{ca} - \omega_2), \tag{2.100}$$

$$\beta_{ab} = -\gamma + i\omega_{ab} + i\delta, \tag{2.101}$$

the Bloch equations of the system become

$$\dot{\sigma}_{cc} = -(\gamma + \Gamma_0)\sigma_{cc} + i(\Omega_2^*\sigma_{ca}^* - \Omega_2\sigma_{ca}) + i(\Omega_1^*\sigma_{cb}^* - \Omega_1\sigma_{cb}), \tag{2.102}$$

$$\dot{\sigma}_{aa} = \gamma\sigma_{aa}^0 + \gamma_{ca}\sigma_{cc} - \gamma\sigma_{aa} + i(\Omega_2\sigma_{ca} - \Omega_2^*\sigma_{ca}^*), \tag{2.103}$$

$$\dot{\sigma}_{bb} = \gamma\sigma_{bb}^0 + \gamma_{cb}\sigma_{cc} - \gamma\sigma_{bb} + i(\Omega_1\sigma_{cb} - \Omega_1^*\sigma_{cb}^*), \tag{2.104}$$

$$\dot{\sigma}_{ca} = \beta_{ca}\sigma_{ca} + i\Omega_2^*(\sigma_{aa} - \sigma_{cc}) + i\Omega_1^*\sigma_{ab}^*, \tag{2.105}$$

$$\dot{\sigma}_{cb} = \beta_{cb}\sigma_{cb} + i\Omega_2^*\sigma_{ab} + i\Omega_1^*(\sigma_{bb} - \sigma_{cc}), \tag{2.106}$$

$$\dot{\sigma}_{ab} = \beta_{ab}\sigma_{ab} + i\Omega_2\sigma_{cb} - i\Omega_1^*\sigma_{ca}^*. \tag{2.107}$$

2.3.3 Adiabatic elimination of the excited state

In order to facilitate the calculation to produce a simpler model of the relevant three-level system, we consider that both pump and probe fields are far detuned from the atomic resonance. The result of this consideration is that $\Delta >> \Gamma_0$ and $\sigma_{cc} \approx 0$. We also assume that the system will be at a stationary state ($\dot{\sigma}_{ij} = 0$). Then, the OBE that should be solved are

$$0 = i(\Omega_2^*\sigma_{ca}^* - \Omega_2\sigma_{ca}) + i(\Omega_1^*\sigma_{cb}^* - \Omega_1\sigma_{cb}), \tag{2.108}$$

$$0 = \gamma(\sigma_{aa}^0 - \sigma_{aa}) + i(\Omega_2\sigma_{ca} - \Omega_2^*\sigma_{ca}^*), \tag{2.109}$$

$$0 = \gamma(\sigma_{bb}^0 - \sigma_{bb}) + i(\Omega_1\sigma_{cb} - \Omega_1^*\sigma_{cb}^*), \tag{2.110}$$

$$0 = i\Delta\sigma_{ca} + i\Omega_2^*\sigma_{aa} + i\Omega_1^*\sigma_{ab}^*, \tag{2.111}$$

$$0 = i\Delta\sigma_{cb} + i\Omega_2^*\sigma_{ab} + i\Omega_1^*\sigma_{bb}, \tag{2.112}$$

$$0 = -\gamma\sigma_{ab} + i\Delta_r\sigma_{ab} + i\Omega_2\sigma_{cb} - i\Omega_1^*\sigma_{ca}^*. \tag{2.113}$$

The following assumptions and definitions were made

$$\Delta = \omega_{ca} - \omega_2, \tag{2.114}$$

$$\Delta_0 = \omega_b - \omega_a, \tag{2.115}$$

$$\Delta_r = \delta + \Delta_0, \tag{2.116}$$

$$\beta_{ca} \approx \beta_{cb} \approx i\Delta, \tag{2.117}$$

$$\beta_{ab} \approx -\gamma + i\Delta_r. \tag{2.118}$$

From 2.111 and 2.112

$$\sigma_{ca} = -\frac{\Omega_2^* \sigma_{aa} + \Omega_1^* \sigma_{ab}^*}{\Delta}, \tag{2.119}$$

$$\sigma_{cb} = -\frac{\Omega_1^* \sigma_{bb} + \Omega_2^* \sigma_{ab}}{\Delta}. \tag{2.120}$$

Inserting 2.119 and 2.120 in 2.113, 2.109, 2.110, and defining $\Omega_R = \frac{\Omega_1^* \Omega_2}{\Delta}$ as the effective Rabi frequency, we obtain

$$0 = \sigma_{ab}[-\gamma + i\Delta_r + i\frac{|\Omega_1|^2 - |\Omega_2|^2}{\Delta}] + i\Omega_R(\sigma_{aa} - \sigma_{bb}), \tag{2.121}$$

$$0 = \gamma(\sigma_{aa}^0 - \sigma_{aa}) - i\Omega_R \sigma_{ab}^* + i\Omega_R^* \sigma_{ab}, \tag{2.122}$$

$$0 = \gamma(\sigma_{bb}^0 - \sigma_{bb}) - i\Omega_R^* \sigma_{ab} + i\Omega_R \sigma_{ab}^*. \tag{2.123}$$

Using 2.121 and the assumption that $\frac{|\Omega_2|^2 - |\Omega_1|^2}{\Delta} << \Gamma << |\Omega_R|$ lead to

$$\sigma_{ab} = \frac{\Omega_R(\sigma_{aa} - \sigma_{bb})(i\gamma - \Delta_r)}{\gamma^2 + \Delta_r^2}. \tag{2.124}$$

Subtracting 2.123 from 2.122, results in

$$(\sigma_{aa} - \sigma_{bb}) = \frac{(\sigma_{aa}^0 - \sigma_{bb}^0)(\gamma^2 + \Delta_r^2)}{\gamma^2 + \Delta_r^2 + 4|\Omega_R|^2}. \tag{2.125}$$

Substituting 2.125 in 2.124, we find that

$$\sigma_{ab} = \frac{\Omega_R(\sigma_{aa}^0 - \sigma_{bb}^0)(i\gamma - \Delta_r)}{\gamma^2 + \Delta_r^2 + 4|\Omega_R|^2}. \tag{2.126}$$

This result will be very useful in the development of chapter 3, where a simple theory will be introduced in order to explain the experimental results shown in chapter 2. And it is important to notice that it depends not only of the Rabi frequencies of the beams, the detuning between the fields, and γ, but also of the difference of the population of the two ground states.

3 FORWARD FOUR-WAVE MIXING VIA RECOIL-INDUCED RESONANCES: EXPERIMENT

Absorption and emission of radiation by atoms give rise to exchange of energy and momentum between an atomic medium and the electromagnetic field due to the recoil of the atoms. If the atoms are sufficiently cold, near Doppler limit, this effect can lead to the appearance of a narrow and dispersive feature in the transmission of a probe beam in a pump-probe experiment. These recoil-induced resonances (RIR) observed in nonlinear spectroscopy were first introduced theoretically by Guo *et al* [6]. Experimental observation occurred two years later in the transmission of a weak probe beam incident in an ensemble of cold atoms in the presence of a one-dimensional optical molasses and making a small angle with a pump beam [5].

RIR has already been used in many applications, from the diagnosis of a working MOT and a 1D optical lattice, by Gawlik *et al* [25, 26], to the storage of light information, by de Almeida *et al* [27]. More recently, it was related to the observation of a giant-gain of a probe beam [28].

In this chapter the fundamentals of RIR will be described. RIR are ultranarrow resonances that require the usage of external degrees of freedom of the atoms to be explained. The explanation to the appearance of this kind of resonances in pump-probe experiments will be done in conjunction with a simple calculation that allows us to associate the energy difference between external degrees of freedom of the atom with the atomic momentum in one specific spatial direction. This relation will also be used in the next chapter to theoretically model the results that will be presented at the end of this chapter.

Another theoretical interpretation of RIR can be given, it is possible to derive some properties of the resonance and of the four-wave mixing signals considering that a pump-probe experiment in an ensemble of cold atoms can be described in terms of Bragg diffraction. This approach will also be qualitatively explained in this chapter.

The first chapter was used to introduce the MOT and the simplified experimental configuration that led to its implementation. In this chapter the experimental details that led to the MOT used to perform the experiments in this work will be shown and briefly explained. The experimental scheme (spatial configuration of the beams, their intensities, detectors, timing, etc.) will be shown and explained.

To finish the chapter, the experimental results will be presented. The RIR and

FFWM spectra were recorded, for different intensities of the pump beam, and will be presented together for comparison.

3.1 FORWARD FOUR-WAVE MIXING VIA RECOIL-INDUCED RESONANCES

3.1.1 Recoil-induced resonances

Usually atoms are at temperatures at which their velocity distribution is large enough to neglect the effect of the variation of atomic velocity due to emission or absorption of radiation. This holds, for example, considering the spectroscopy of atomic vapors (hot atoms). However, when atoms are at temperatures near Doppler limit, the effect of photon recoil velocity ($v_R = \frac{k\hbar}{m}$) is not negligible. Under this situation, the different center-of-mass momentum states of the atom needs to be considered. A phenomenon analogous to the Raman process between internal atomic states now takes place involving transitions between external momentum states.

It will be considered the scheme depicted in figure 8, a pump-probe experiment in a cold atom ensemble, with $\theta \approx 1°$. An atom can absorb from the pump beam (beam with direction defined by $\vec{k}_2$) and emit into the probe (beam with direction defined by $\vec{k}_1$) direction, like in 8a, or absorb from the probe beam and emit into the pump direction (figure 8b). The first situation results in the amplification of the probe beam and the second in the attenuation of the probe beam.

As the atomic center-of-mass momentum states are now considered, the energy levels of the atoms become a product of internal and external degrees of freedom. The Raman processes that give rise to the phenomena presented in figure 8a and 8b are illustrated in 8c and 8d, considering the external degrees of freedom of the atom.

To our purposes, the momentum distribution of the atoms follows a Maxwell-Boltzmann distribution. This means that the population of a state decreases as the modulus of the momentum is increased. This difference in the population is essential for the appearance of RIR, because both phenomena (amplification and absorption of probe beam) are occurring at the same time between different pairs of states, the difference between states' population makes one process overcomes the other.

To mathematically model the system, we should calculate the changing in the kinetic energy of an atom after the interaction with the fields. The initial momentum of the atom in the y direction is p_y and the wavevectors of the fields are given by

$$\vec{k_2} = k\hat{z}, \tag{3.1}$$

Figure 8: Pump-probe experiment resulting in the amplification of the probe beam (a) or attenuation of probe beam (b), and Raman processes between external energy levels of the atoms, that result in the (c) amplification of the probe beam and (d) attenuation of probe beam.

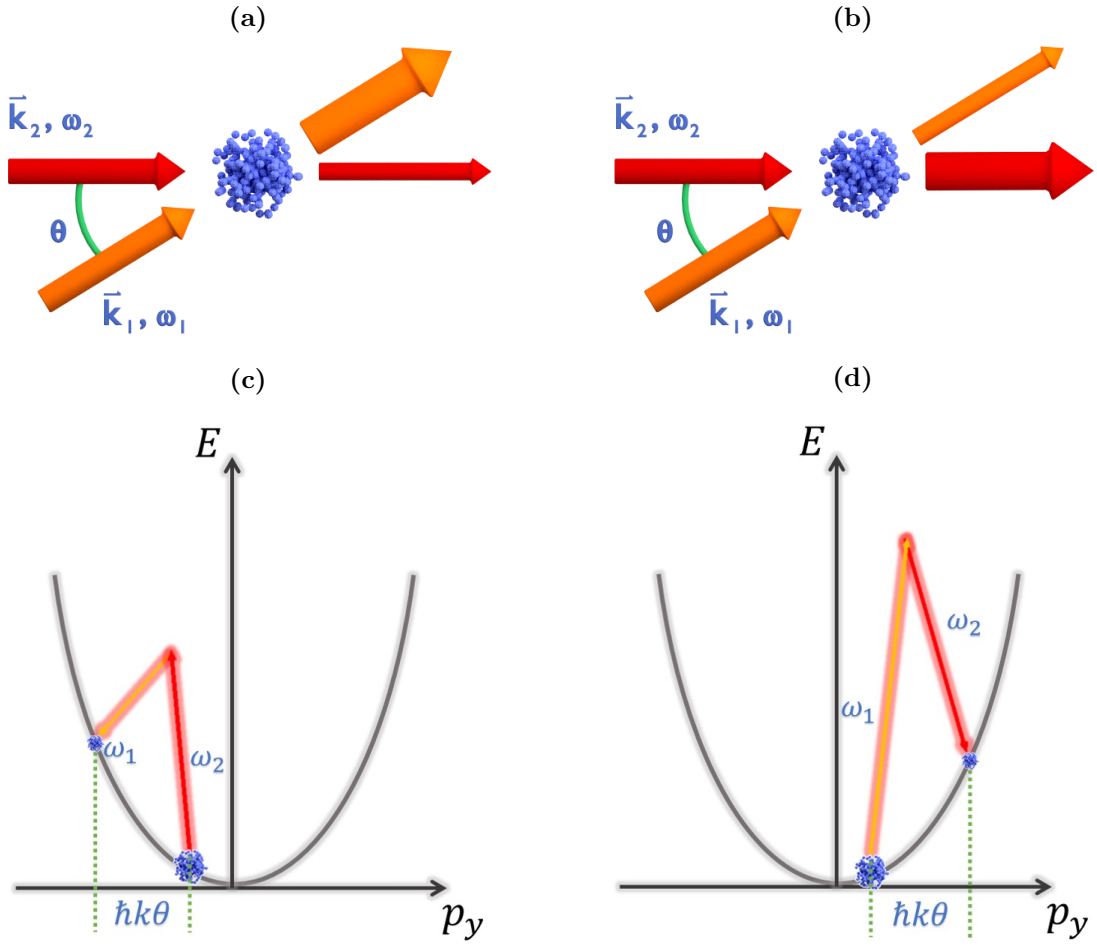

Source: Modified from [19].

$$\vec{k_1} = k(cos(\theta)\hat{z} + sin(\theta)\hat{y}). \tag{3.2}$$

As $\theta \approx 0$, we can consider $\vec{k_1} = k(\hat{z} + \theta\hat{y})$. In the situation that an amplification of the probe occurs, the change in the atom's momentum is given by

$$\Delta\vec{p} = \hbar(\vec{k_2} - \vec{k_1}) = -\hbar\theta k\hat{y}. \tag{3.3}$$

The final momentum of the atom is

$$p_f = p_y - \hbar\theta k. \tag{3.4}$$

Conservation of energy leads to

$$\frac{p_f^2}{2m} = -\hbar\omega_b + \hbar\omega_a - \frac{p_y^2}{2m}, \tag{3.5}$$

then

$$0 = \frac{\hbar^2 k^2 \theta^2}{2m} - \frac{p_y \hbar k \theta}{m} + \hbar\Delta_0. \tag{3.6}$$

As $p_y >> 2k\theta\hbar$

$$\Delta_0 \approx \frac{p_y k \theta}{m}, \tag{3.7}$$

this result will be used to calculate the transmission spectrum of the probe beam and the lineshape of the respective forward four-wave mixing signal in the next section.

3.1.2 Four-wave mixing via RIR

The nonlinear interaction between the laser fields and the cold atomic ensemble can be used to produce beams in directions different than the propagation's direction of the incident beams. This occurs, for example, due to four-wave mixing processes described in 2.2.1. In the situation depicted in figure 9, the two incident fields interact with the nonlinear medium that has a considerable $\chi^{(3)}$, giving rise to a field in the direction of $2\vec{k}_2 - \vec{k}_1$. This is the field that was measured together with the transmission of the probe beam. The experimental details will appear in the next sections of this chapter.

Figure 9: Incidence of two beams in a nonlinear atomic medium, generating one additional field in the direction defined by $2\vec{k}_2 - \vec{k}_1$.

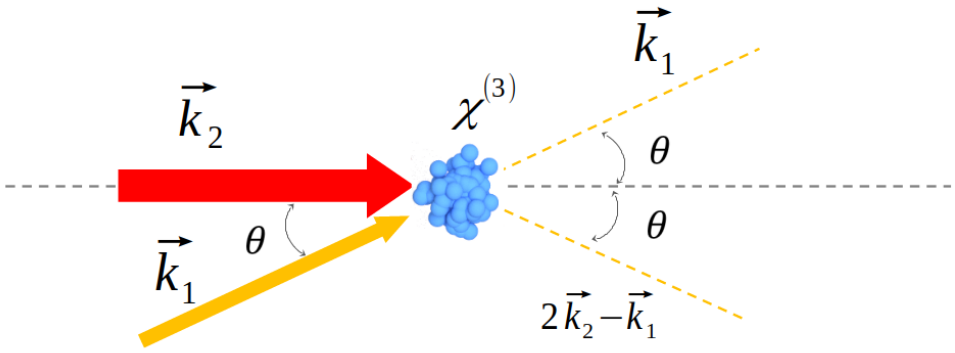

Source: The author (2019).

In terms of a parametric process, the generation of four-wave mixing via RIR can be explained as an extension of the process shown in 8c, and can be seen in figure 10. After the effective emission in the $\vec{k}_1$ direction, another absorption from the pump field can occur, followed by an emission of a field with frequency defined by $\omega_D = 2\omega_2 - \omega_1$. This process is known in the literature as forward four-wave mixing (FFWM). Although the existence of the FFWM signal via RIR is predictable, its measurement has not been reported before. The main reason must be the effectivity of this process in comparison with other four-wave mixing processes that can arise from RIR. As can be seen at 2.59, the FFWM does not fulfill the phase-matching condition.

Figure 10: Raman transitions between external degrees of freedom that represent the FFWM generation.

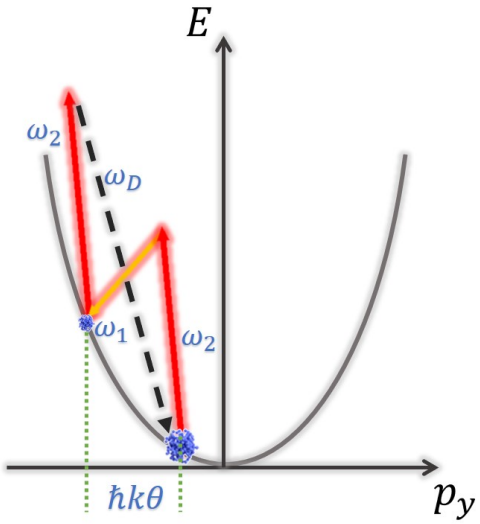

Source: The author (2019).

3.1.3 Bragg's diffraction interpretation

Another physical qualitative interpretation of this phenomenon arises from the well-known Bragg's law, very important in x-ray crystallography, for example. The requisite for the validity of Bragg's law is that the wavelength of the incident wave must be smaller than two times the spacing between parallel atomic planes. More on diffraction of waves by periodic structures can be found in [29].

In the propagation of two beams in an atomic medium, like the one shown in the figure 9, the beams interfere creating a periodic intensity pattern. Consequently, a diffraction grating of atomic density stem. To describe the grating, one can define a vector called "grating's vector" as $\vec{G} = \vec{k}_2 - \vec{k}_1$, this vector defines the direction of light the intensity pattern formed in the medium. It can be shown [30] that the spatial period of this grating is given by $\Lambda = \frac{2\pi}{|\vec{G}|}$, the velocity of the grating is $v = \frac{\delta}{|\vec{G}|}$ and, as the wavelength of the fields are much smaller than the period of the grating $(1, 7.10^{-2}\Lambda = \lambda)$, where λ is the wavelength of the fields, Bragg's diffraction condition is accomplished. This corresponding intensity pattern will trap the atoms at the region of maximum intensity due to the dipole force described before, thus creating a density grating which can diffract the incident beams. Therefore, two fields can be generated in the directions defined by Bragg's diffraction law $\vec{k}_g = \vec{k}_2 \pm \vec{G}$, where $\vec{k}_g$ denotes the wavevectors of the diffracted fields. One of the fields propagates along the probe's direction and the other propagates along the FFWM direction. The illustration of this process is shown in figure 11.

The gain and absorption in the direction of the probe's transmission, explained in the last subsection, can be explained, from this perspective, as an interference between the

Figure 11: Representation of Bragg's diffraction of the pump beam in a grating of density of atoms created by pump and probe beams.

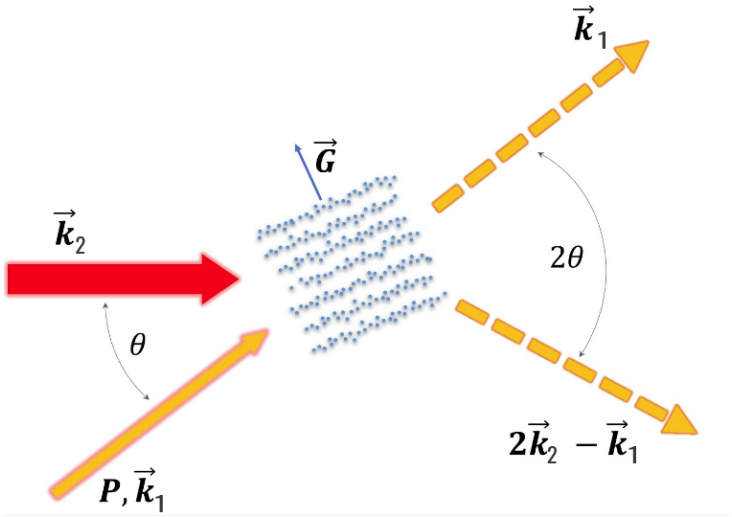

Source: Modified from [7].

probe beam and the diffraction of the pump beam along the probe's direction. Because the atomic medium has a finite response time, there is a phase delay between the diffracted field and the incident probe so the interference can be constructive or destructive. If $\delta < 0$ the two beams interfere constructively resulting in the amplification of the probe beam, and if $\delta > 0$ the two beams interfere destructively resulting in the attenuation of the probe beam. At $\delta = 0$ the grating is stationary, the situation is symmetric, and there is no net amplification or attenuation either of the probe or the pump.

3.2 EXPERIMENTAL APPARATUS

3.2.1 The MOT

Three pairs of counterpropagating laser beams red-detuned by 12 MHz with respect to the transition $F = 4 \leftrightarrow F' = 5$ of the D_2 line of ^{133}Cs were used to obtain a MOT as described in section 2.1 and to perform the experiment that will be detailed next. This transition is a "closed transition", because according to the selection rules presented in 2.1.1, as long as the atom is excited to the level $F' = 5$ it can only decay to the level $F = 4$. But there is also a nonzero probability that the MOT beams also excite the atoms to $F' = 4$. Consequently, the atoms can decay to the noninteracting level $F = 3$. To avoid this effect, two other pairs of counterpropagating laser beams were introduced in resonance with the transition $F = 3 \leftrightarrow F' = 4$, this beams are called "repump beams". The effect of the MOT and repump beams in the population of the atoms with respect to the relevant hyperfine levels is illustrated in the figure 12. The spatial gradient of magnetic field is

introduced by a pair of coils in anti-Helmholtz configuration.

Figure 12: D_2 line of ^{133}Cs including the effect of the MOT and repump beams.

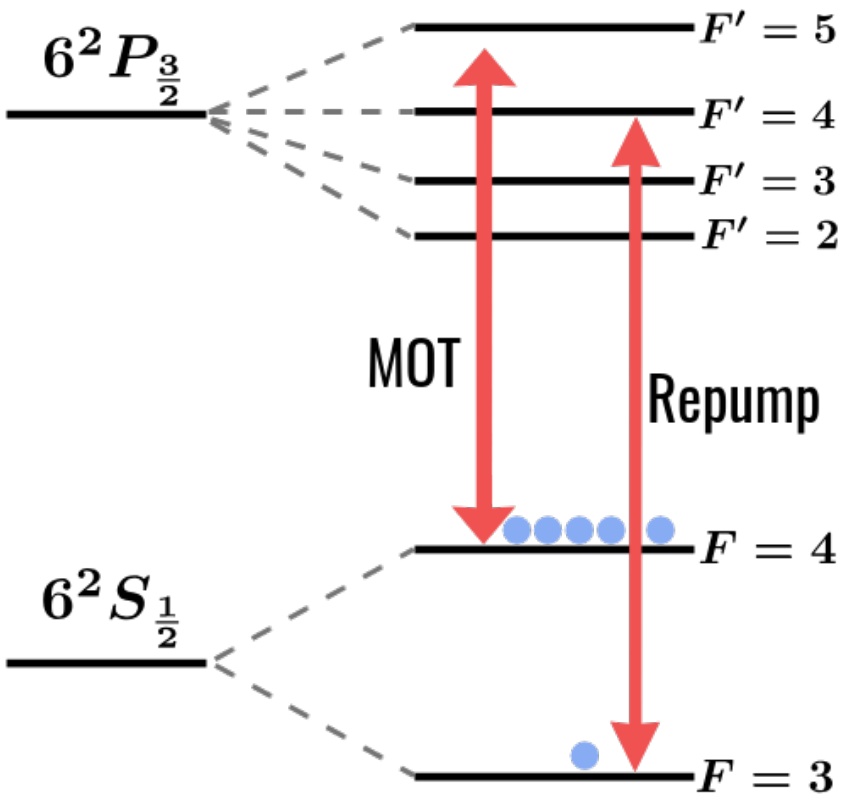

Source: The author (2019).

It is also interesting to guarantee that no external magnetic field is being applied to the system, as it would break the degeneracy of the hyperfine sublevels, introducing effects that are not desired. This is done by the application of a compensating magnetic field produced by three pairs of coils in Helmholtz configuration, one in each spatial direction (the current applied to each pair is independent). We use radio frequency (RF) spectroscopy to monitor the populations and the Zeeman shift of each sublevel, which allow us to cancel the magnetic field in the cold sample, as described next.

Initially the system is prepared in the hyperfine level $F = 4$ and the frequency of the RF field is varied near the resonance frequency between the hyperfine ground state levels $F = 4$ and $F = 3$. Depending on the orientation of the antenna; π transitions, σ transitions or even both can be induced. A probe field is then applied to the cloud. This probe is nearly resonant with the frequency of the transition $F = 4 \leftrightarrow F' = 5$. The RF field is applied for 150 μs, 10 μs before the probe field. If it is almost resonant to transitions between magnetic sublevels of the hyperfine levels $F = 4$ and $F = 3$, it would change the population of the sublevels of $F = 4$, resulting in a decay in the absorption of the probe field. The transmission of the probe is measured as a function of the RF

frequencies, and, if there is an external magnetic field, the peaks corresponding to Zeeman transitions are seen (the number of peaks depends on the type of transitions induced). If the magnetic field is almost cancelled, only one peak is seen, because the Zeeman sublevels are almost degenerated. This technique allows us to guarantee that the external magnetic field is cancelled with a resolution of the order of 5 mG. More on this technique can be found in [7, 31]. All the measurements were performed in a MOT with optical depth of the order of 3.

3.2.2 Experimental configuration for the measurement of RIR and FFWM signal

The theoretical and experimental basis of the present work were introduced in the previous sections. They correspond to topics already covered in the literature, either in books, articles or thesis. Hereafter, the novelty of this work will be highlighted, which is the experimental observation of FFWM via RIR. Specifically the experimental configuration that was used will be detailed, in order to provide a better understanding of the results that will be shown in the end of the chapter.

Figure 13: Experimental configuration representing the optical path of the laser beams until the atomic medium that generates the signals monitored by the two detectors (D_1 and D_2).

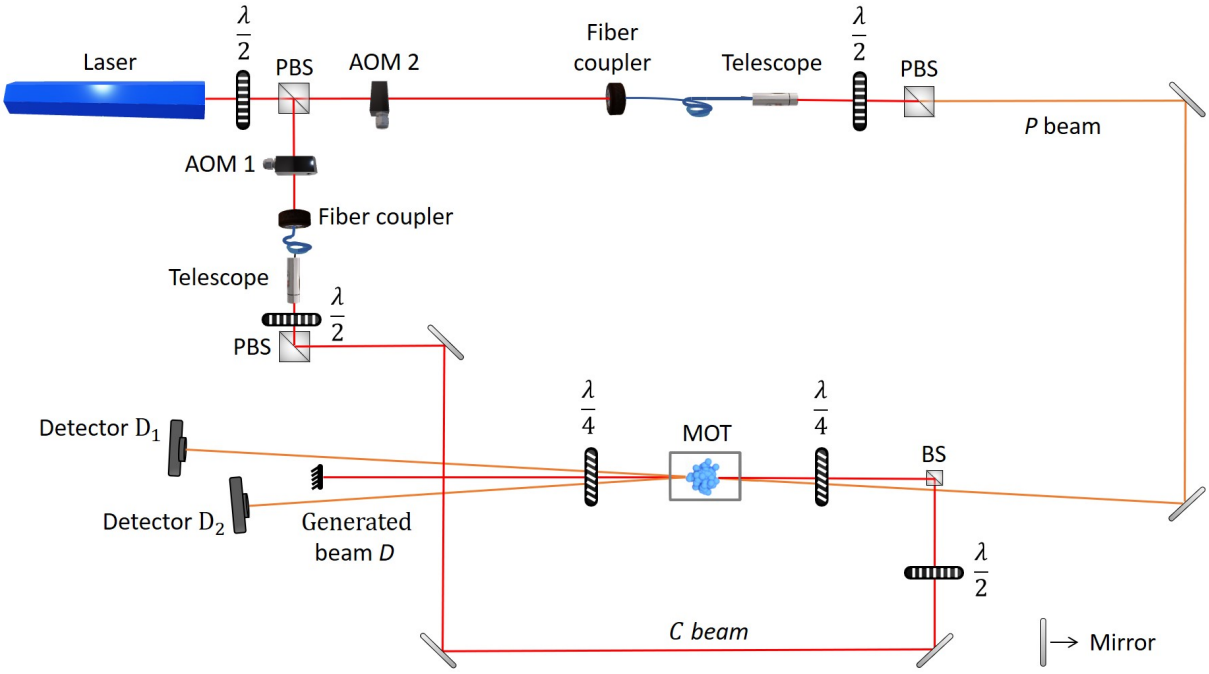

Source: Modified from [7].

The experimental configuration of the system is depicted in figure 13. We use a

Toptica laser (model DL100) emitting in 852 nm. The laser was locked using the saturated absorption technique [16] in the *crossover* resonance associated with the transitions $F = 4 \leftrightarrow F' = 4$ and $F = 4 \leftrightarrow F' = 5$. Then, the beam is splitted by a PBS (Polarizing beam splitter) after passing through a half-wave plate. The pump beam (C) has its frequency red-detuned by 6Γ ($\frac{\Gamma}{2\pi} \approx 5.2$ MHz) from the $F = 4 \leftrightarrow F' = 5$ transition by an acousto-optic modulator (AOM 1) to finally couple to a fiber, and then has its intensity controled by a combination of half-wave plate and PBS. Before its interaction with the atomic ensemble, it passes, consecutively, through a half-wave plate, a beam splitter and a quarter-wave plate in order to change its polarization to σ^+ according to our convention. The path of the probe beam is similar. The AOM 2 is used to vary the frequency of the probe beam (P) with respect to the frequency of the C beam, it also passes through a half-wave plate and a PBS to control its power, and finally it also has its polarization changed to σ^+ before reaching the cloud. The two telescopes were used to collimate the beams. The detector D_1 was used to measure the transmission of the P beam and the detector D_2 to measure the FFWM signal.

To facilitate the understanding of the physical processes involved in the present work, from this point on, all the optical technicalities will be neglected and when the experimental scheme will be mentioned it will refer to the very simplified figure 14. The angle used between C and P was $\theta = 1°$.

Figure 14: Simplified experimental configuration illustrating the interaction between the beams (C and P) and the atomic cloud. The generated signals are monitored by the detectors D_1 and D_2.

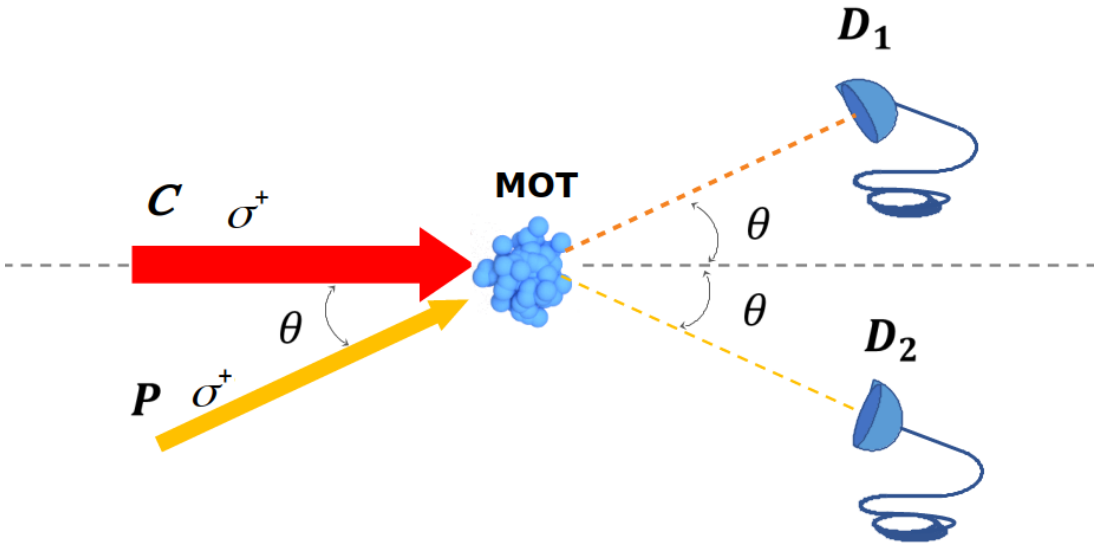

Source: Modified from [7].

As both beams excite the atomic cloud with σ^+ polarization, we can consider that the atoms are pumped to the sublevel $F = 4$, $m_F = +4$. This occurs because, by

selection rules, a σ^+ field can only induce transitions with $\Delta m_F = 1$. This effect allows us to interpret the interaction between the beams and the atoms as just the interaction of two fields and a pure two-level system (not considering, by now, the atomic external degrees of freedom). As mentioned before, the external magnetic field was cancelled, so the interaction between the laser fields and the atoms is as illustrated in figure 15.

Figure 15: Interaction of a σ^+ polarized field and the $F = 4 \leftrightarrow F' = 5$ transition of the D_2 line of ^{133}Cs, resulting in the pumping of the atoms to the magnetic sublevel $m_F = 4$ of the hyperfine level $F = 4$.

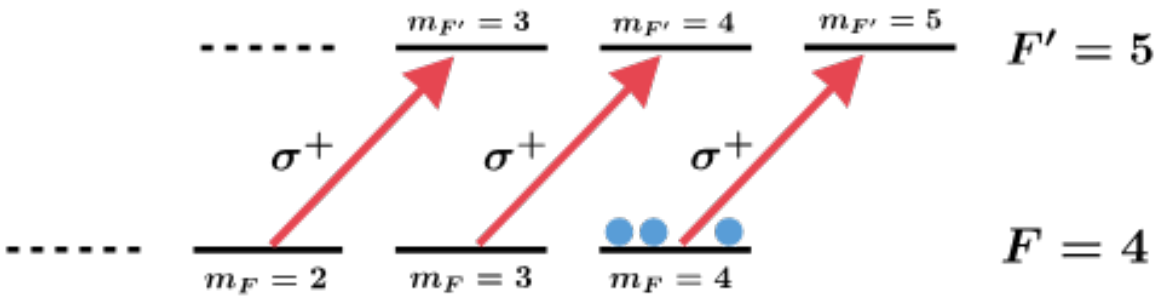

Source: The author (2019).

Finally, the theoretical explanation of the results that will be presented at this chapter can be done by just considering the interaction of two fields and two-level systems (represented in 16), when considering only the internal degrees of freedom of the atom.

3.2.3 Time sequence of the experiment

The complete experiment is managed by a multifunction module from *National Instruments*, of the series PCI-6133. It has a temporal resolution of 100 ns. The module and a *Labview* software were used to control the timing of the beams used in the MOT, the beams used to perform the experiment and also the magnetic fields. This temporal control of the experiment is very important, because one needs to turn off the beams of the MOT as well as the MOT magnetic field while the experiment is being performed. The interaction of the beams of the experiment with the beams of the MOT would make the analysis of the experiment very difficult. A very interesting study on RIR in an operating MOT was done by Gawlik *et al* [25]. In the present case the analisys presented in Gawlik's work is not needed, because we can perform the experiment with no additional field.

Figure 17 illustrates the temporal sequence of the experiment. At first, the MOT and the repump beams are turned on at the same time. After 20 ms the MOT beams are turned off and the repump beams remain turned on for more 1 ms. This guarantees that the atoms will be pumped to the $F = 4$ level, as described before. The experiment

Figure 16: Interaction of the pump and probe fields with a pure two-level system.

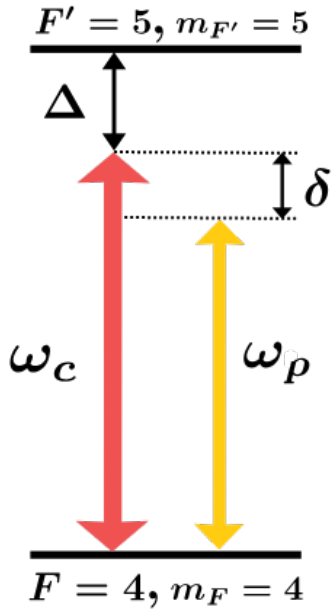

Source: The author (2019).

is performed during 800 μs, 0.2 ms after the repump beams were turn off, this delay is necessary to certify that the magnetic field of the MOT is zero.

Figure 17: Temporal sequence for the realization of the experiment.

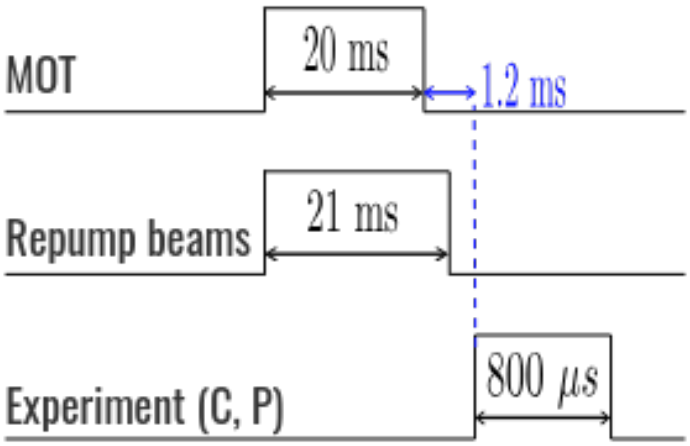

Source: The author (2019).

3.3 RESULTS

The experiment is performed in 800 μs, during the time C and P are on. It consists in measuring the probe's transmission and the FFWM signal as the frequency of the probe beam is varied with respect to the pump's frequency. This change in the probe's frequency is done by an acousto-optic modulator (AOM 2) and an *Agilent* function generator, the function generator introduces a voltage in the modulator of the AOM in steps of 125 μV (which corresponds to a change of 1.15 kHz in the probe's frequency). The intensity of the probe beam was fixed during the experiment and its value was 0.2 $\frac{mW}{cm^2}$, while the pump's intensity was varied in the range from 7 $\frac{mW}{cm^2}$ to 37 $\frac{mW}{cm^2}$.

3.3.1 Transmission Spectrum and FFWM signal

Avalanche photodectors (APDs) detect the probe's tansmission and the FFWM signal for 800 μs. The FFWM amplitude as a function of time, for $\delta = 0$, is shown in figure 18. The signals are integrated for 30 μs starting at 700 μs, i.e. near its maximum value, and the sets of the integration's results for all measured values of δ are represented in figure 19, for both probe's transmission and FFWM signal.

Figure 18: Dependence of the amplitude of FFWM signal on time, for pump-probe detuning of $\delta = 0$.

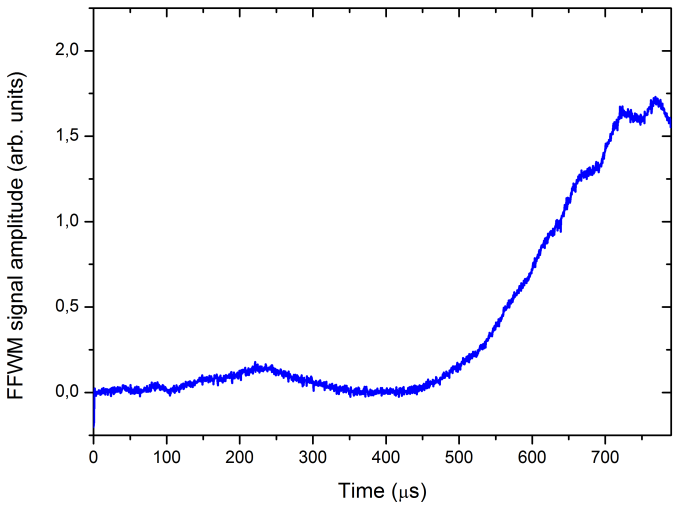

Source: The author (2019).

In figure 19 we show the probe transmission and the FFWM spectra for three different pump intensities (11, 14 and 25 $\frac{mW}{cm^2}$) . The transmissions clearly represent recoil-induced resonances, the dispersive lineshape and the distance between the two peaks are

Figure 19: Transmission spectrum (in black) and FFWM signal (in blue) for intensities of the pump beam of (a) 11 $\frac{mW}{cm^2}$, (b) 14 $\frac{mW}{cm^2}$ and (c) 25 $\frac{mW}{cm^2}$.

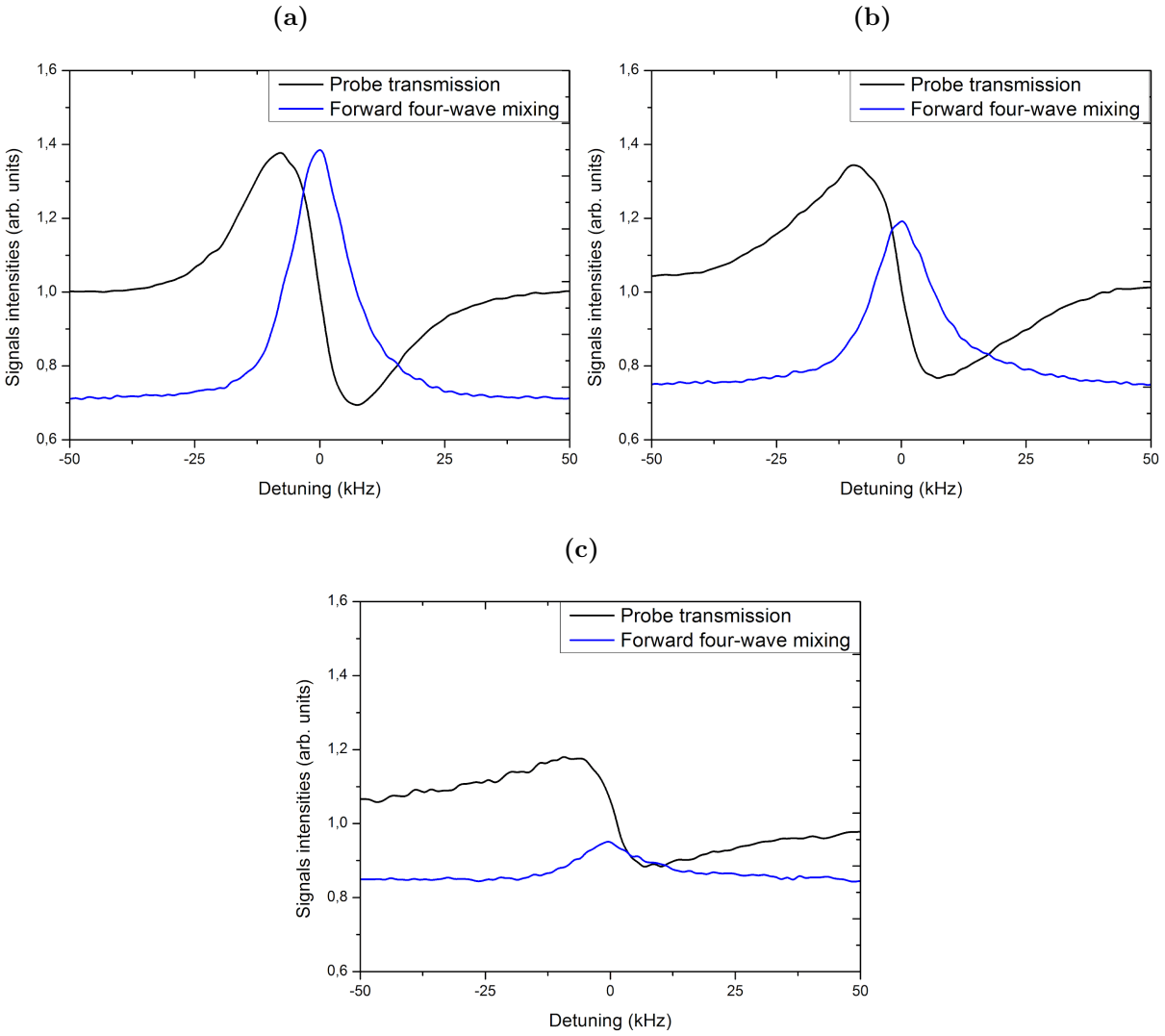

Source: The author (2019).

compatible with this resonance [5]. The FFWM signals have their maximum values when the pump-probe detuning is zero and their width are similar to the transmission signal. The transmission signal and the generated signal are in different scales, so no comparisons between their amplitudes can be inferred from the figures. However, for the situation of maximum amplitude of the FFWM observed, the reflectivity of the process (defined as the intensity of the generated signal over the intensity of the probe beam) was 30 %.

The goal of the next chapter is to theoretically reproduce the lineshapes presented in figure 19 by a simple model using the OBE for the interaction of two fields and an effective three-level system.

3.3.2 Dependence of the signals with respect to pump's power

Figure 20: Amplitude of the FFWM signal for different intensities of the pump beam.

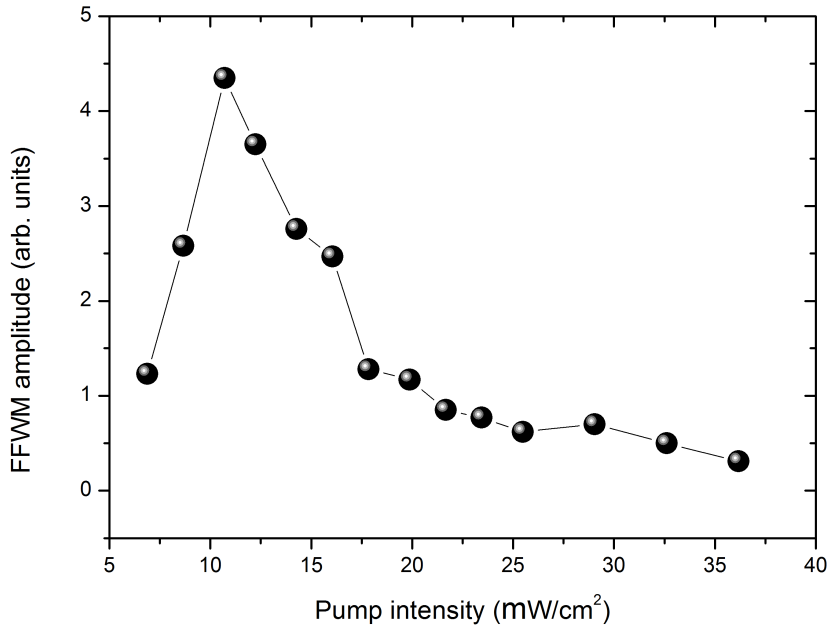

Source: The author (2019).

The experiment was performed for 14 different intensities of the pump beam, the limitation is the resolution of the FFWM signal. As the intensity of the pump beam is increased; for small values of intensity, the amplitude of the FFWM increases. However, this process rapidly saturates and then the amplitude decays (as can be seen in 20). One possible cause of this behaviour might be a mechanical effect of the light in the cloud of atoms. As the two incident beams are copropagating, due to radiation pressure they push the cloud, and this may lower the effectivity of the wave-mixing process.

Full width at half maximum (FWHM) of the FFWM signal was also measured for different pump intensities, and the result is depicted in figure 21.

Figure 21: Full width at half maximum of the FFWM signal for different intensities of the pump beam.

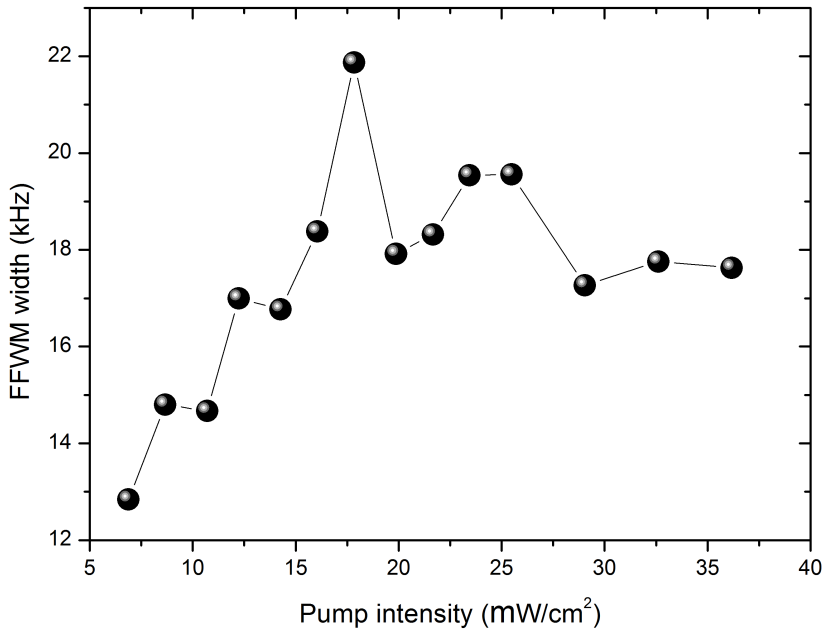

Source: The author (2019).

4 FORWARD FOUR-WAVE MIXING VIA RECOIL-INDUCED RESONANCES: A SIMPLE THEORETICAL MODEL

The purpose of the present chapter is to develop a simple theoretical model to reproduce the lineshape of the signals presented in chapter 2. The development of such a simple model is possible, because for σ^+ polarized pump beam it can be considered that the internal structure of the cesium atoms are simply two-level systems, as shown in 16.

Recoil-induced resonances result from atom-light interactions when the atomic recoil due to the absorption-emission process becomes not negligible. Therefore, the external degrees of freedom of the atoms should be considered and processes like the one shown in figure 8 are allowed. In order to model the previously explained experiment it should be considered that the light fields induce transitions between levels that are a tensorial product of internal and external degrees of freedom.

This chapter is divided in two sections: in the first one, a theoretical model based on the results obtained in section 2.3 will be introduced and developed to explain the lineshapes observed for RIR and FFWM. The second section compares the model with a result that is already present in the literature [32], that demonstrates that RIR can be used to measure the temperature of the atomic ensemble, to guarantee that this model is compatible to what is expected from previous results.

4.1 THEORETICAL MODEL

As can be seen in figure 10, four different momentum states are necessary to explain the appearance of a FFWM signal via RIR in such pump-probe experiment. Then, as the internal structure of the atoms can be considered as a simple two-level system and the atomic energy levels should be a tensorial product of internal and external levels, we consider the interaction of pump and probe fields with a four-level system. The relevant levels, depicted in figure 22, consists of two states that are products of the internal excited state with different momentum states and two that are products of the internal ground state with two other different momentum states.

The model assumes that both fields interact with the system, creating a coherence between levels $|g, \vec{p}_i\rangle$ and $|g, \vec{p}_i + \hbar(\vec{k}_2 - \vec{k}_1)\rangle$, in a process called "writing process". After the creation of this coherence, we assume that the atoms interact again with the pump

Figure 22: Representation of the interaction between 2 fields and a four-level system, where the energy levels are tensorial products of internal and external atomic degrees of freedom.

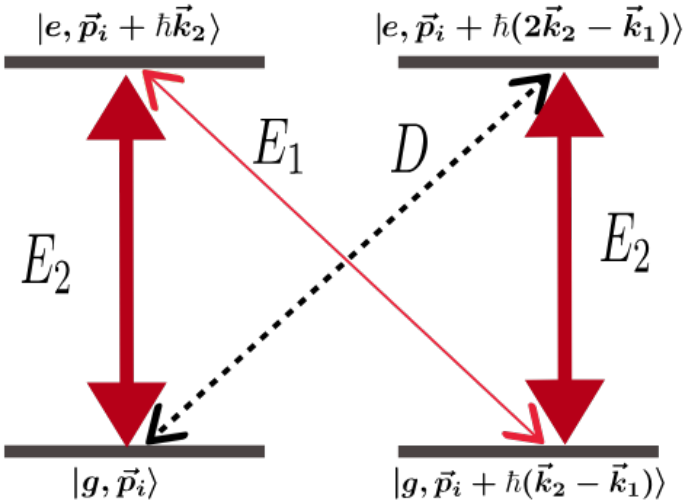

Source: The author (2019).

beam, generating coherences between excited and ground states, in the "reading process". These coherences will be related to both probe's transmission and FFWM signal by the results given in the section 2.2.

It is important to emphasize that there is no time delay between writing and reading processes, they occur simultaneously. This nomenclature just emphasizes that the coherence between the two ground states was created (written) by the interaction of the system with both fields, and used to generate (read) the optical relevant coherences. These processes will be explained in more details in the continuity of the chapter. To perform the exact solution of the problem one should have considered the OBE of the four-level system coupled with two fields. The model is just a simplification and it is not intended to explain the process in its totality.

4.1.1 Writing process

The writing process is represented in figure 23. From now on, generic states will be considered representing the states depicted in 22. The pump field couples with the $|a\rangle \leftrightarrow |c\rangle$ transition and the probe field couples withe the $|b\rangle \leftrightarrow |c\rangle$ transition. At this point, as stated before, we want to know the coherence between the two ground states, i.e. σ_{ab}. This system is totally analogous to the one considered in section 2.3. As the pump beam was detuned by 6Γ from the relevant transition in the experiment, the adiabatic elimination of the excited state can be performed. Therefore, the notation used in section

Figure 23: Representation of the writing process.

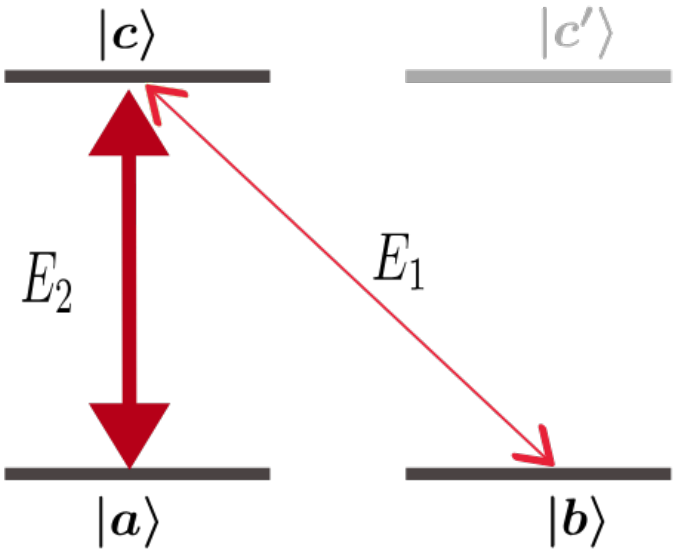

Source: The author (2019).

2.3 will be maintained.

As a result of the writing process, already calculated in 2.3, the coherence $\sigma_{ab}(p_y)$ is given by

$$\sigma_{ab}(p_y) = \frac{\Omega_R(\sigma^0_{aa} - \sigma^0_{bb})(i\gamma - \Delta_r)}{\gamma^2 + \Delta_r^2 + 4|\Omega_R|^2}. \tag{4.1}$$

Where

$$\Delta_r = \delta + \Delta_0, \tag{4.2}$$

$$\Omega_R = \frac{\Omega_1^* \Omega_2}{\Delta}, \tag{4.3}$$

$$\Delta_0 \approx \frac{p_y k \theta}{m}, \tag{4.4}$$

and γ is related to the rate of atoms that enter and leave the region of interaction with the lasers, as defined in 2.3.2.

4.1.2 Reading process

The reading process consists in a second interaction of the pump beam and atomic system, considering that the coherence σ_{ab} was already created in the writing process. This process can occur in two different ways: the first one is the coupling of the pump beam with the $|a\rangle \leftrightarrow |c\rangle$ transition again, and the other is the coupling of the pump beam with the $|b\rangle \leftrightarrow |c'\rangle$ transition.

Figure 24: Reading process responsible for the generation of (a) σ_{cb} and (b) $\sigma_{c'a}$.

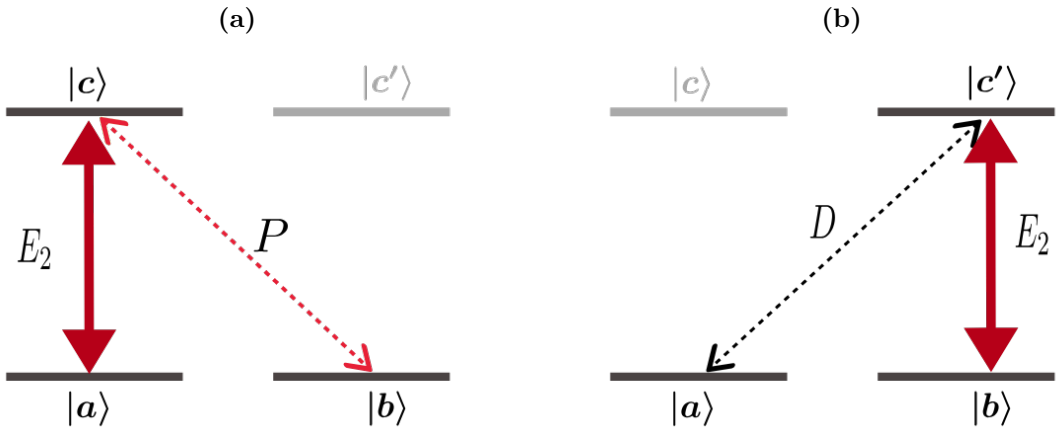

Source: The author (2019).

When the pump field couples with the $|a\rangle \leftrightarrow |c\rangle$ transition (as can be seen in figure 24a), a coherence σ_{cb} is created. The absorption coefficient of the atomic medium, as calculated in section 2.2, is proportional to the imaginary part of σ_{cb}. In order to calculate $\sigma_{cb}(p_y)$ one needs to consider the OBE for the Λ system, but the only coupling is between pump field and the transition $|a\rangle \leftrightarrow |c\rangle$. 2.120 and 4.1 results in

$$\sigma_{cb}(p_y) = \frac{\Omega_2^* \Omega_R (\sigma_{aa}^0 - \sigma_{bb}^0)(-i\gamma + \Delta_r)}{\Delta(\gamma^2 + \Delta_r^2 + 4|\Omega_R|^2)}. \tag{4.5}$$

σ_{cb} depends on p_y because Δ_r depends on p_y by 3.7, and also $(\sigma_{aa}^0 - \sigma_{bb}^0)$ depends on the momentum distribution of the ensemble. σ_{aa} and σ_{bb} represent the population of the internal ground state with momentum p_y and $p_y + \hbar(\vec{k}_2 - \vec{k}_1)$, respectively. In order to find the total coherence one needs to perform an integration of 4.5 over all momentum states. Thus,

$$\mathrm{Im}\,\sigma_{cb} = \Omega_2^* \Omega_R \gamma \int_{-\infty}^{\infty} \frac{(\pi[p_y + \Delta p_y] - \pi[p_y])}{(\gamma^2 + \Delta_r^2 + 4|\Omega_R|^2)\Delta} dp_y. \tag{4.6}$$

$\pi[p_y]$ is an integrable and smooth function that describes the population's distribution over the momentum states. If Δp_y is small, one can approximate $\frac{\partial \pi(p_y)}{\partial p_y} \approx \frac{(\pi[p_y + \Delta p_y] - \pi[p_y])}{\Delta p_y}$, then the expression 4.6 becomes

$$\mathrm{Im}\,\sigma_{cb} = \Omega_2^* \Omega_R \gamma \int_{-\infty}^{\infty} \frac{\Delta p_y}{(\gamma^2 + \Delta_r^2 + 4|\Omega_R|^2)\Delta} \frac{\partial \pi(p_y)}{\partial p_y} dp_y. \tag{4.7}$$

Assuming that the atomic momentum distribution follows a Maxwell-Boltzmann distribution, i.e.,

$$\pi(p_y) = \frac{m}{\sqrt{2\pi} p_u} e^{\frac{-p_y^2}{2p_u^2}}, \tag{4.8}$$

where m is the mass of the atom and p_u is the average momentum of the atoms of the ensemble, given by $p_u = \sqrt{mk_BT}$, 4.7 becomes

$$\mathrm{Im}\,\sigma_{cb} = -\frac{\Omega_2^*\Omega_R\gamma}{\sqrt{2\pi}p_u^3}\int_{-\infty}^{\infty}\frac{\hbar k\theta p_y m e^{-\frac{p_y^2}{2p_u^2}}}{(\gamma^2+(\delta+\Delta_0)^2+4|\Omega_R|^2)\Delta}dp_y. \tag{4.9}$$

The probe transmission spectrum is the result of the integral 4.6 propagated through the medium by $e^{-\frac{\alpha}{2}z}$, where α is proportional to the imaginary part of σ_{cb}, as shown in 2.2.2. The direction of the field is defined implicitly in the term $\Omega_2^*\Omega_R$ that includes the direction of the incident waves ($\vec{k}_1$ and $\vec{k}_2$) and the result is proportional to Ω_1^*, then the resulting wave propagates through the direction of incidence of the probe beam.

In addition to the coupling of the pump beam with the transition $|c\rangle \leftrightarrow |b\rangle$, it can also couple with the transition $|b\rangle \leftrightarrow |c'\rangle$ (represented in figure 24b) in the reading process, giving rise to a coherence $\sigma_{c'a}$, which will generate the field propagating along the direction $2\vec{k}_2 - \vec{k}_1$. In section 2.2 it was shown that the intensity of the generated field is proportional to the modulus squared of the relevant coherence. To compute $\sigma_{c'a}(p_y)$ one should solve the OBE calculated in section 2.3, neglecting the coupling of the probe beam, using 4.1. The resulting coherence is

$$\sigma_{c'a}(p_y) = \frac{\Omega_2^*\Omega_R^*(\sigma_{aa}^0-\sigma_{bb}^0)(i\gamma+\Delta_r)}{\Delta(\gamma^2+\Delta_r^2+4|\Omega_R|^2)}. \tag{4.10}$$

Following the same procedure used for $\sigma_{cb}(p_y)$, the expression for the total coherence, $\sigma_{c'a}(p_y)$, integrated over all momentum states is

$$\sigma_{c'a} = \frac{\Omega_2^*\Omega_R^*}{\sqrt{2\pi}p_u^3}\int_{-\infty}^{\infty}\frac{\hbar k\theta p_y m e^{-\frac{p_y^2}{2p_u^2}}(-i\gamma+\delta+\Delta_0)}{(\gamma^2+(\delta+\Delta_0)^2+4|\Omega_R|^2)\Delta}dp_y. \tag{4.11}$$

The FFWM signal can be obtained by using 4.11 and remembering that its intensity is proportional to $|\sigma_{c'a}|^2$. The direction of the generated field is defined implicitly in the term $\Omega_2^*\Omega_R*$ that includes the direction of the incident waves ($\vec{k}_1$ and $\vec{k}_2$), then its direction is defined by the wavevector proportional to $2\vec{k}_2 - \vec{k}_1$.

It is also important to notice that the difference between the states' population is indispensable to the appearance of RIR, as noticed in chapter 2. In the present model this requirement is explicit in 2.124, if $\sigma_{aa} = \sigma_{bb}$ then $\sigma_{ab} = 0$. Therefore, all of the coherences calculated in the present section would have been equal to zero.

4.1.3 Theoretical results

In order to theoretically obtain the transmission and FFWM spectra, we have to integrate equations 4.9 and 4.11. A numerical integration using the software *Mathematica*

Figure 25: Theoretically obtained lineshape for (a) probe transmission, where can be seen a gain for $\delta < 0$ and attenuation for $\delta > 0$; and (b) FFWM signal, that is maximum at $\delta = 0$. The calculations were performed using as parameters' values: $\gamma = 2 \times 10^3$ Hz, $\Omega_R = 1.5 \times 10^6$ Hz and a mean velocity of 10 $\frac{cm}{s}$.

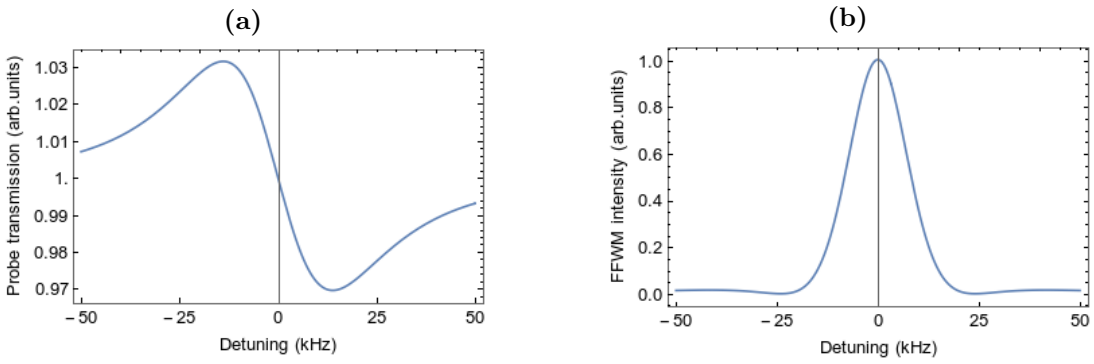

Source: The author (2019).

was performed for both signals and using parameters' values similar to their values in the experiment, we show in figure 25 the calculated lineshape in the limit $\gamma << \Omega_R$.

The developed model is very simple; but as can be seen if figure 25, its results are very similar and compatible with the measured lineshapes depicted in 19. However, due to the simple nature of the model, it does not explain the dependence of the FFWM width with respect to pump's intensity.

4.2 VELOCIMETRY OF COLD ATOMS VIA RIR

4.2.1 Velocimetry via transmission signal

To check the validity of a model it is useful to compare its results with results already known from literature. It was shown that RIR can be used to measure the velocity distribution of the atoms in a MOT [32]. They demonstrate that the distance between the maximum and minimum points of the RIR signal is given by (defining u as the mean velocity of the atoms)

$$\delta_{RIR} = 2k\theta u, \tag{4.12}$$

To obtain 4.12 in our model, we assume that the system is in the regime of low intensities ($\Omega_R << \gamma$). Therefore, the integral 4.9 becomes a product of a Lorentzian function centered at $p_y = -\frac{\delta m}{k\theta}$, and the derivative of a Gaussian function.

In the limit $\gamma << \frac{k\theta p_u}{m}$, the Lorentzian function represents a Dirac delta function,

then 4.9 becomes

$$\operatorname{Im}\sigma_{cb} = \frac{\Omega_2^*\Omega_R}{\Delta}\frac{\hbar\delta e^{-\frac{\delta^2}{2(k\theta u)^2}}}{\sqrt{\pi}uk_BT}. \tag{4.13}$$

That is just the derivative of a Gaussian function. Expression 4.12 is obtained by finding the maximum and minimum points of 4.13.

The numerical integration of 4.9 in the low intensities regime also reproduces 4.12, as shown in figure 26.

Figure 26: Theoretical dependence of the transmission width, with respect to the atomic mean velocity.

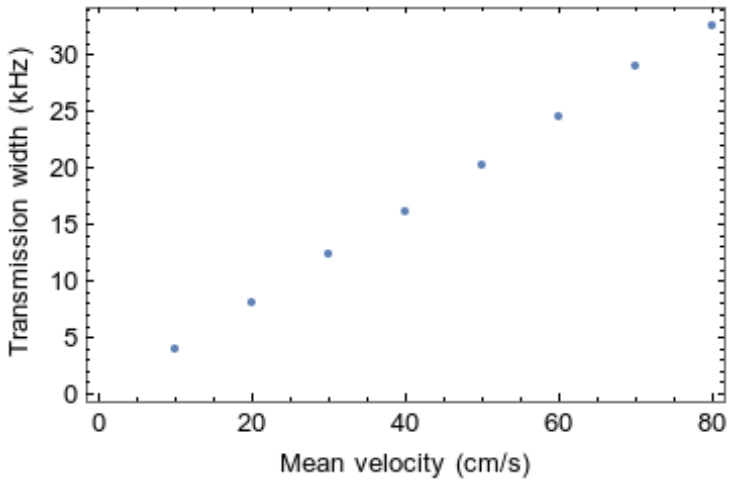

Source: The author (2019).

4.2.2 Velocimetry via four-wave mixing signal

To find a simple expression like 4.12 for the FFWM width is not possible, due to the difficulty in solving exactly the integral 4.11. Even in the low intensities regime, approximation of the Lorentzian function to a Dirac delta function cannot be performed for the real part of $\sigma_{c'b}$, because $\operatorname{Re}\sigma_{cb}$ is exactly zero in the center of the Lorentzian.

However, numerical results indicate that the FFWM signal can be used to estimate the mean velocity of the atomic cloud. The relation between FFWM width at half maximum and the atomic mean velocity is also linear, as shown in 27.

An application of this result could be the use of FFWM via RIR as an alternative to the transmission signal, to estimate the temperature of atoms trapped in a MOT.

Figure 27: Theoretical dependence of the FFWM width, with respect to the atomic mean velocity.

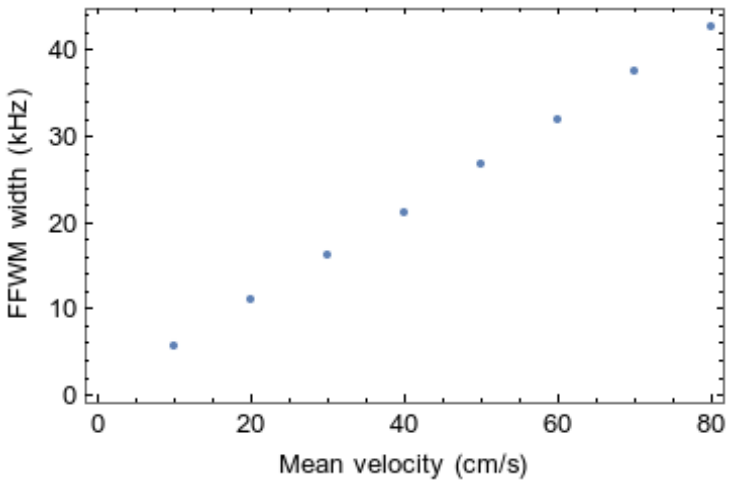

Source: The author (2019).

5 CONCLUSION

In this work, FFWM via RIR was observed in an experiment performed in an ensemble of cold cesium atoms. The atoms were trapped by a magneto-optical trap, and initially prepared in the $F = 4$ hyperfine level of the atomic ground state. The observation was done by the incidence of two beams in the atomic ensemble; the beams were circularly polarized with parallel polarizations, with respect to each other, and red detuned to the $F = 4 \leftrightarrow F' = 5$ transition of cesium's D_2 line.

In the experiment, pump and probe beams with wavevectors $\vec{k}_2$ and $\vec{k}_1$respectively, are incident in a sample of cold atoms and the probe beam transmission is detected simultaneously with the generated FWM beam propagating along the direction $2\vec{k}_2 - \vec{k}_1$. The observed spectra clearly reveal the characteristics of RIR.

We also studied the dependence of the FFWM spectral signal with respect to pump's power. It shows that the signal's width increases with pump's intensity, for low intensities, until saturates. The signal's amplitude also increases for small intensities, but rapidly reaches a maximum value to then decay.

The experimental conditions are the simplest possible to the observation of RIR, allowing us to consider the internal atomic structure as a two-level system. Therefore, the signals' lineshapes were theoretically reproduced by a simple model that mathematically just requires the solution of the optical Bloch equations for a three-level system interacting with two electromagnetic fields. The model consists in separating the complete parametric process responsible for the generation of FFWM, in two steps. The first one named *writing process* and the second named *reading process*. The writing process is the interaction of the two fields with the atomic system, creating a coherence between atomic states; and the second process just considers the interaction of the system with the pump beam making use of the coherence created before.

Finally, a comparison between the developed model and a result alread present in the literature was performed to guarantee its validity, and conjecture the possibility of using FFWM via RIR to measure the temperature of MOTs.

The perspectives of continuity of the present work are foccused on using the measured signals to detect squeezed states of light between two distinct modes, generated by a four-wave mixing process related to recoil-induced resonances. Although squeezed states between the probe's transmission and a four-wave mixing signal generated by atom-light interaction were already measured before, they were not related to transitions between atomic momentum states, which shows specific characteristics as reported in [27].

BIBLIOGRAPHY

[1] M. H. Anderson, J. R. Ensher, M. R. Matthews, C. E. Wieman, E. A. Cornell, *Science* **269**, 198-201 (1995).

[2] K. B. Davis, M. -O. Mewes, M. R. Andrews, N. J. van Druten, D. S. Durfee, D. M. Kurn, and W. Ketterle, *Phys. Rev. Lett.* **75**, 3969 (1995).

[3] T. H. MAIMAN, *Nature* **187**, 493–494 (1960).

[4] E. L. Raab, M. Prentiss, Alex Cable, Steven Chu, and D. E. Pritchard, *Phys. Rev. Lett.* **59**, 2631 (1987).

[5] J.-Y. Courtois, G. Grynberg, B. Lounis, and P. Verkerk, *Phys. Rev. Lett.* **72**, 3017 (1994).

[6] J. Guo, P. R. Berman, B. Dubetsky, and G. Grynberg, *Phys. Rev. A* **46**, 1426 (1992).

[7] Jesús Pavón López, *PhD thesis, UFPE* (2019).

[8] C. F. McCormick, A. M. Marino, V. Boyer, and P. D. Lett, *Phys. Rev. A* **78**, 043816 (2008).

[9] M. Brune, F. Schmidt-Kaler, A. Maali, J. Dreyer, E. Hagley, J. M. Raimond, and S. Haroche, *Phys. Rev. Lett.* **76**, 1800 (1996).

[10] H. J. Kimble, *Nature* **453**, 1023–1030 (2008).

[11] Immanuel Bloch, Jean Dalibard and Sylvain Nascimbène, *Nature Physics* **8**, 267–276 (2012).

[12] J. J. Sakurai and Jim Napolitano. Modern Quantum Mechanics, *Cambridge University Press* (2017).

[13] Ramamurti Shankar. Principles of Quantum Mechanics, *Springer* (2011).

[14] T. Hänsch and A. Schawlow, *Opt. Comm.* **13**, 68 (1975).

[15] Andreev, S., V. Balykin, V. Letokhov, and V. Minogin, *JETP Lett.* **34**, 442 (1981).

[16] Foot, Christopher J. Atomic Physics, *Oxford University Press* (2005).

[17] Steck, Daniel A. *Cesium D line data* (2003).

[18] Boyd, Robert W. Nonlinear Optics, *Elsevier* (2003).

[19] Allan Johnes Ferreira de Almeida, *PhD thesis, UFPE* (2018).

[20] Hélène Perrin, *Les Houches lectures on laser cooling and trapping* (2003).

[21] Yariv, A. Quantum Electronics, *Wiley* (1989).

[22] J. R. R. Leite, P. Simoneau, D. Bloch, S. Le Boiteux and M. Ducloy, *Europhys. Lett.* **2**, 747 (1986).

[23] D. Felinto, D. Moretti, R. A. de Oliveira, and J. W. R. Tabosa, *Optics Lett.* **35**, 3937 (2010).

[24] Steven Chu, L. Hollberg, J. E. Bjorkholm, Alex Cable, and A. Ashkin, *Phys. Rev. Lett.* **55**, 48 (1985).

[25] Tomasz M. Brzozowski, Maria Brzozowska, Jerzy Zachorowski, Michał Zawada, and Wojciech Gawlik, *Phys. Rev. A* **71**, 013401 (1994).

[26] Maria Brzozowska, Tomasz M. Brzozowski, Jerzy Zachorowski, and Wojciech Gawlik, *Phys. Rev. A* **73**, 063414 (1994).

[27] A. J. F. de Almeida, M.-A. Maynard, C. Banerjee, D. Felinto, F. Goldfarb, and J. W. R. Tabosa, *Phys. Rev. A* **94**, 063834 (2016).

[28] J. P. Lopez, A. M. G. de Melo, D. Felinto, and J. W. R. Tabosa, *Phys. Rev. A* **100**, 023839 (2019).

[29] Charles Kittel. Introduction to Solid State Physics, *Wiley* (2004).

[30] Christine Triche. *PhD Thesis, École Polytechnique X.* (1997).

[31] Marcia Frómeta Fernández *Master's thesis, UFPE* (2019).

[32] D. R. Meacher, D. Boiron, H. Metcalf, C. Salomon, and G. Grynberg, *Phys. Rev. A* **50**, R1992(R) (1994).